Energy dissipated by concrete barriers in vehicle impact scenarios by combined numerical and analytical approaches

By

Isaac Klugh

B.S., Kansas State University, 2018

A THESIS

submitted in partial fulfillment of the requirements for the degree

MASTER OF SCIENCE

Department of Civil Engineering
College of Engineering

KANSAS STATE UNIVERSITY
Manhattan, Kansas

2020

Approved by:

Major Professor
Dr. Hayder Rasheed

Copyright

Abstract

The American Association of State Highway Transportation Officials (AASHTO) LRFD Bridge Design Specifications requires that bridge piers be capable of withstanding a lateral 600 kip static force. Older, bridge piers throughout Kansas, specifically those constructed before the requirement for the 600 kip force was established, often have insufficient load resistance. Any changes to a bridge require the piers to meet modern requirements in the AASHTO code so pavement replacement can require pier retrofits. Compared to a complete structural overhaul of the existing piers, protective concrete barriers may provide a cost, and time, effective approach to help piers meet current code requirements. Currently, no standards are available to reduce the magnitude of the lateral force requirement through the use of barriers. By combining yield line analysis and finite element analysis, this thesis establishes a baseline for the energy absorbed by a concrete barrier. A combination of various angles of impact, initial vehicle velocities and barrier boundary conditions are considered to build an envelope of scenarios. The results of this research show the vehicle's kinetic energy and velocity may reduce by up to 57% and 35%, respectively, for a large truck.

Acknowledgements

I would like to thank my major professor, Dr. Hayder Rasheed, for his support throughout my undergraduate and graduate career. His passion for structural engineering has always been an inspiration and source of ambition. I would also like to thank Dr. Christopher Jones for his high level of dedication and guidance provided throughout this research project. Lastly, I would like to thank Dr. Krishna Ghimire for his willingness to join my Advisory Committee on short notice.

Table of Contents

List of Figures

List of Tables

Chapter 1: Introduction

Section 1.1: Problem Statement

AASHTO code requires bridge piers be designed to withstand a lateral load of 600 kips static force to account for a vehicle collision. This value, provided in AASHTO [1], is based on results from the Texas Transportation Institute (TTI) [2 & 3]. Older bridge piers in the jurisdiction of the Kansas Department of Transportation (KDOT) are often inadequate for the modern requirement. Any changes to a bridge require the piers to meet modern requirements in the AASHTO code, so pavement replacement, for example, can require pier retrofits. Compared to a complete structural overhaul of the existing piers, protective concrete barriers may provide a cost, and time, effective approach to help piers meet current code requirements. While many studies, such as Zain [4], Badiee [5], and Calloway [6], have aimed to determine a more accurate ultimate force of concrete barriers, little research has investigated the energy absorbed by the barrier and the effect on the pier collision force after traversing the protective barrier. This study will focus on a specific barrier design provided by KDOT and currently in use (Figure 1.1) and results may vary for other designs. Note that this study uses a simplified geometry represented by the solid lines; the dashed lines show the actual geometry. The objective of this study is to quantify the change in vehicle energy before the pier collision and justify a reduction to the required 600 kip static force through the use of protective barriers.

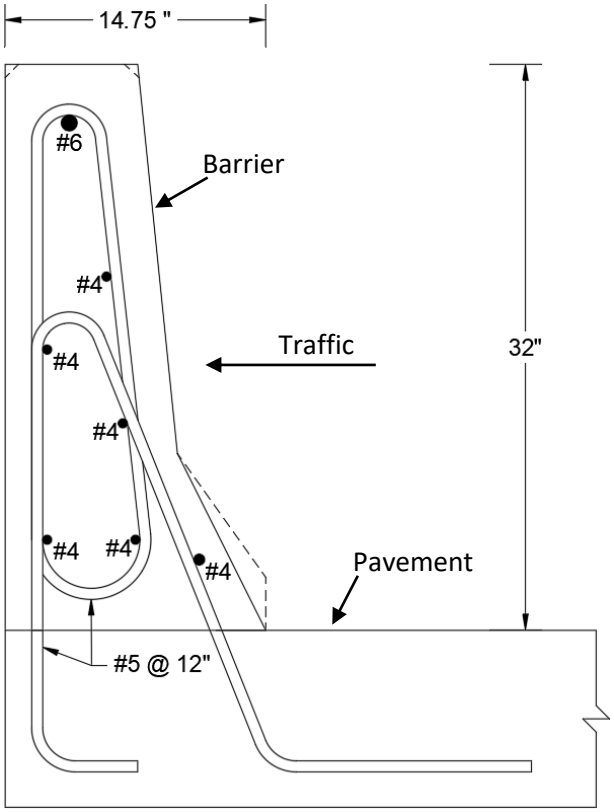

Figure 1.1: Cross-section of barrier design provided by KDOT

Section 1.2: Background on 600 kips

Before Buth's 2010 and 2011 reports [2&3], the design specifications required piers be designed to resist a 400 kip transverse load rather than the current 600 kip load. After studying a collection of crash data, analyzing bridge pier impact scenarios through finite element analysis (FEA), and collecting empirical data of the forces experienced during full-scale impacts, the TTI research team recommended raising the required load to 600 kips. An 80 kip tractor-trailer truck was selected as the design vehicle for the specification. The simulations used a fully rigid column while the experimental tests used a highly rigid column. There is evidence that these columns may overestimate the necessary design force.

Section 1.3: Analysis Approach

This thesis combines transient dynamic FEA, static FEA, and yield line analysis to verify results and develop a more confident estimate of the energy dissipated by concrete jersey barriers. Yield line analysis provides an estimate of the required static force to fail the barrier, but does not directly provide values for the energy absorbed in the process. Combining yield line analysis with static FEA, in Abaqus software, allows for an approximation of the energy absorbed by the barrier. Implementing a separate approach with transient dynamic FEA in LS-DYNA results in a more extensive dataset of 20 collision scenarios and a direct time-history for both energy and velocity during the simulation. The results of transient dynamic FEA can be more easily compared with, or used by, independent sources for result validation. The comparison of transient dynamic FEA with the combined yield line analysis and static FEA allows for further validation of results.

Chapter 2: Literature Reviews

The following literature review includes a brief progression of pier design specifications, protective barrier guidelines, crash statistics and risk analysis. Changes in the pier design specifications will be covered in Section 2.1. Effects from the design characteristics of piers and vehicles is reviewed in Section 2.2. Section 2.3 will discuss guidelines and analyses of protective barriers. Section 2.4 provides summaries of crash data studies and risk analysis of pier impacts.

Section 2.1: AASHTO Design Specifications

AASHTO's 1992 Standard Specifications for Highway Bridges stated "when possibility of collision exists from highway or river traffic, an appropriate risk analysis should be made to determine the degree of impact resistance to be provided and/or the appropriate protection system" [7]. In the early design guidelines, no exact force was specified for design purposes. However, in 1994, the 1st edition of the AASHTO LRFD Bridge design Specifications, included "abutments and piers located within a distance of 30.0 ft to the edge of a roadway … shall be designed for an equivalent static force of 400 kip" [8]. The 400 kip capacity came from Hirsch in 1985 [9], who used an 80 kip tank truck as the design vehicle. In 1999 the AASHTO Subcommittee on Bridges and Structures ended the Standard Specifications for Highway Bridges [10]. AASHTO and the Federal Highway Administration (FHWA) decided all new components of bridges should be designed according to the AASHTO LRFD Bridge Design Specifications by 2007. Buth's work in 2010 [2] and 2011 [3] led to several changes in the 6th Edition of AASHTO's LRFD Bridge Design Specifications [11]. First, the design load increased from a 400 kip load to a 600 kip load. This change came from the result of full-scale crash test in which the peak force slightly exceed 600 kips for an 80 kip tractor-trailer truck [3]. Additionally, the impact height of the vehicle on the column was raised from 4 feet to 5 feet as observed in the crash test [10] and the angle of impact was narrowed

from any angle to angles between 0° and 15°.The change in angle of approach was based on the analysis of several collections of crash data as discussed in Section 2.4.

Section 2.2: Effects of Pier and Vehicle Designs

Buth [2] is the primary source for the strength of reinforced-concrete piers under impact loading. Buth calculated the shear capacity of nine piers with increasing diameter and reinforcement. The smallest pier, with a diameter of 24 inches, had a calculated shear capacity of only 148 kips. The largest pier, with a diameter of 72 inches, had a calculated shear capacity of 1,366 kips. From the piers that Buth analyzes, the 600 kip requirement was not satisfied until the diameter of the pier was over 48 inches [2]. These calculations suggest that piers with a diameter of 36 inches are likely insufficient for the required capacity. The National Cooperative Highway Research Program (NCHRP) Report 892 [10] explains that these capacities may still be sufficient in some designs where only two piers are required for strength, but a third pier is added for redundancy.

Buth's research also simulated two variations of a single dump truck [2]. In the first, the dump truck was transporting a deformable ballast and the peak forces exceed 2,000 kips. The second variation used the same truck with a rigid ballast. In this simulation, the peak force approximately tripled that of the deformable ballast. Without changing the geometry or mass of the truck, Buth demonstrated that the vehicle characteristics play a major role in the impact forces experienced.

Section 2.3: Guidelines for Protective Barriers

NCHRP Report 230 [12] included the crash testing guidelines for protective barriers up until 1993. In 1993, the publishing of NCHRP Report 350 [13] updated the guidelines to include six different levels for protective longitudinal barriers [10]. Test levels one, two and three covered the performance of barriers

subjected to passenger vehicles such as small cars and pickup trucks. Test levels four, five and six include the vehicles previously covered, as well as large trucks and other heavy vehicles. NCHRP 350 establishes the testing metrics for each test level including vehicle weight, speed, and angle of approach. TL-5 and TL-6 use the 80 kip tractor-trailer trucks used for determination of the required static loads on bridge piers. In 2016, the AASHTO Manual for Assessing Safety Hardware (MASH) [14] was updated to replace NCHRP 350 as the guideline for protective barriers [10]. The exact vehicle characteristics were slightly modified for TL-3 and TL-4 between NCHRP 350 and MASH [10]. According to AASHTO LRFD Bridge Design Specifications, TL-5 barriers should be used to protect piers when required static forces are not considered in the design of those piers [1].

Zain and Mohammed [4] compiled and analyzed data from a large set of studies. While the research objective was to determine the optimized design of a barrier, it provides many useful conclusions. The studies compiled include full scale experiments, scale laboratory tests, finite element analyses and yield line calculations. One significant point of the research finds that for impacts of heavy vehicles, a barrier with a base of 600 mm, top width of 240 mm and height of 813 mm can provide high stability and impact resistance. Additionally, the study also concludes that with an approach angle of 15°, the barrier has a high chance to deflect a vehicle without allowing full penetration. This agrees with the recommendation from AASHTO design specifications [1] and Buth [2]. Zain finds that the laboratory tests often apply static loads perpendicular to the barrier and are therefore less useful or accurate. Full scale tests on the other hand provide more accurate data due to the variation in angles and true high-rate impacts. Finally, a vehicle weight of only 2 tons is used in approximately 55% of the studies reviewed by Zain. As AASHTO specifications are based on a large 80 kip tractor-trailer truck, more research is needed for heavy vehicles.

Badiee [5] performed FEA of impact scenarios between the f800 used in chapter 3 of this thesis and 5 various barrier designs. Badiee suggests that yield line analysis as recommend by AASHTO is a highly conservative approach to finding the maximum load capacity of a concrete barrier. The research includes not only transient dynamic simulations and also static load simulations. Comparing stresses from the static load and the dynamic scenarios, the study concludes that yield line analysis and even static FEA are both inadequate for accurate analysis and design of barriers. Using yield line analysis and static FEA will provide an extremely conservative design for strength while ignoring other failure limits, such as vehicle roll-over. Badiee explains that dynamic FEA allows for the consideration of "vehicle roll-over, vehicle redirection, vehicle damage and motion of the loaded region in steep angles of approach." Combining these effects can have a significant impact on the results of the analysis.

Section 2.4: Crash Data and Risk Analysis

Buth [2] provides most of the analysis of crash data pertaining to heavy vehicles impacting piers. While much of the study is qualitative, the simple quantitative results yield relevant findings. Of the 19 crashes investigated by Buth, 13 resulted in failure of at least one column in the pier system. This clearly demonstrates that many piers currently in use are not designed to the modern standard. The number of columns per pier is not known for every case, but no structures were reported to have only one column in a pier. If only one column is present, then collapse of the bridge is guaranteed. In the cases Buth studied, only five of the bridges failed. Considering the likelihood of a total bridge failure due to a single column failure is an important factor in the risk analysis of a pier impact. While column redundancies are effective, the cost is also much higher. Buth shows that in several cases, the heavy vehicles were able to vault protective barriers or even completely maneuver around protective barriers before striking the piers [2]. This suggests the barriers may be inadequately designed or lack appropriate length to intercept vehicles.

Buth also developed risk probabilities for a bridge pier to be hit depending on the state and type of roadway in question. The results show, for example, a probability of being impacted of 2.19×10^{-8} for divided roads in Minnesota and 1.09×10^{-9} for a divided highway in Texas. Due to the large discrepancy in probabilities, there is no clear value that should be selected for the probability of an impact. Analysis of additional data including other states and road types may develop a more obvious pattern. The probability also ignores characteristics such as the distance between the pier and the road, the presence of protective barriers or regional climate and typical weather conditions [10]. Buth's approach to the probability also only considers the traffic flow of heavy trucks. No consideration is made for the different flows of passenger cars that may increase driving congestion or hazards.

Chapter 3: Transient Dynamic FEA

Section 3.1: Truck Parameters:

For the LS-DYNA simulations, the Ford f800 single unit truck model provided by the National Transportation Research Center, Inc. (NTRCI) [15] was selected (Figure 3.1). This vehicle is widely accepted as a benchmark in vehicle crash studies and the model has been studied and enhanced for realistic collision behaviors. The f800 model contains over 160 materials, primarily elastic-plastic shell elements. Concealed within the cargo area, a ballast mass is located directly behind the truck cab as shown in Figure 3.2. The ballast mass has an elastic modulus approximately half the value of steel and can be considered a rigid payload.

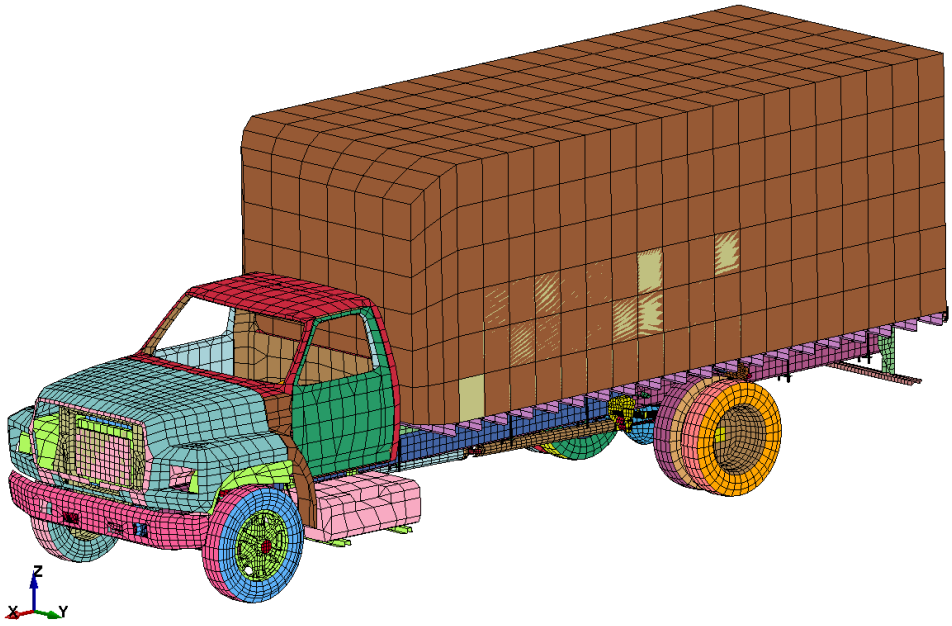

Figure 3.1: Ford f800 model

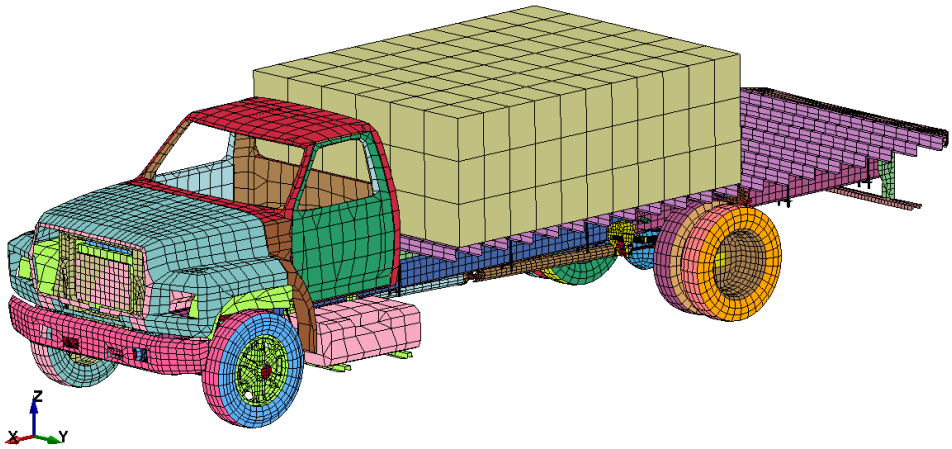

Figure 3.2: Ford f800 ballast payload

Comparing to the models used in the TTI report, the f800 geometry is more similar to the SUT dump truck (Figure 3.3) than the full tractor trailer. Buth created the dump truck by modifying a model of a full tractor-trailer truck. Buth et al. simulated the dump truck colliding with a fully rigid column as shown in Figure 3.4 and created the force-time curve shown in Figure 3.5. To verify the f800 model as a valid vehicle model, the force-time curve is compared to the curve from Buth. Force-time curves for most vehicle impacts can be defined by three significant characteristics: the magnitude of the first peak, the magnitude of the second peak, and the time between the two peaks (Figure 3.5).

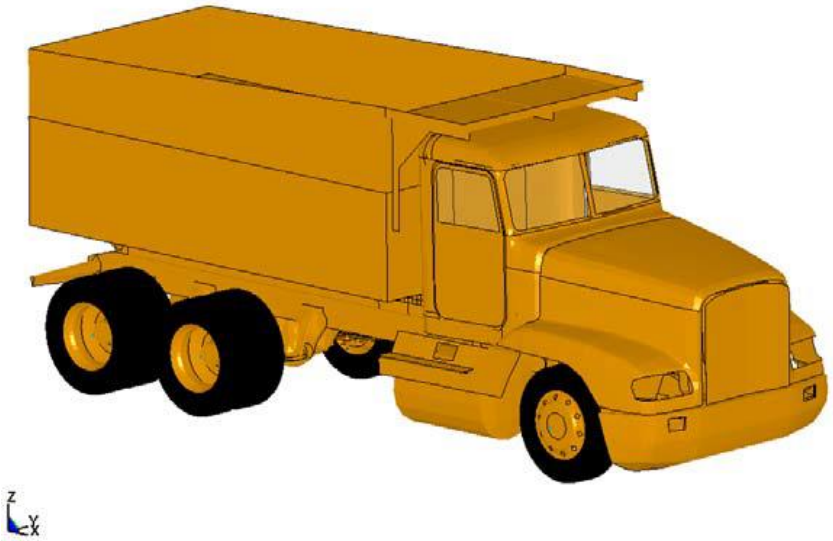

Figure 3.3: SUT rigid ballast dump truck used in TTI research [2]

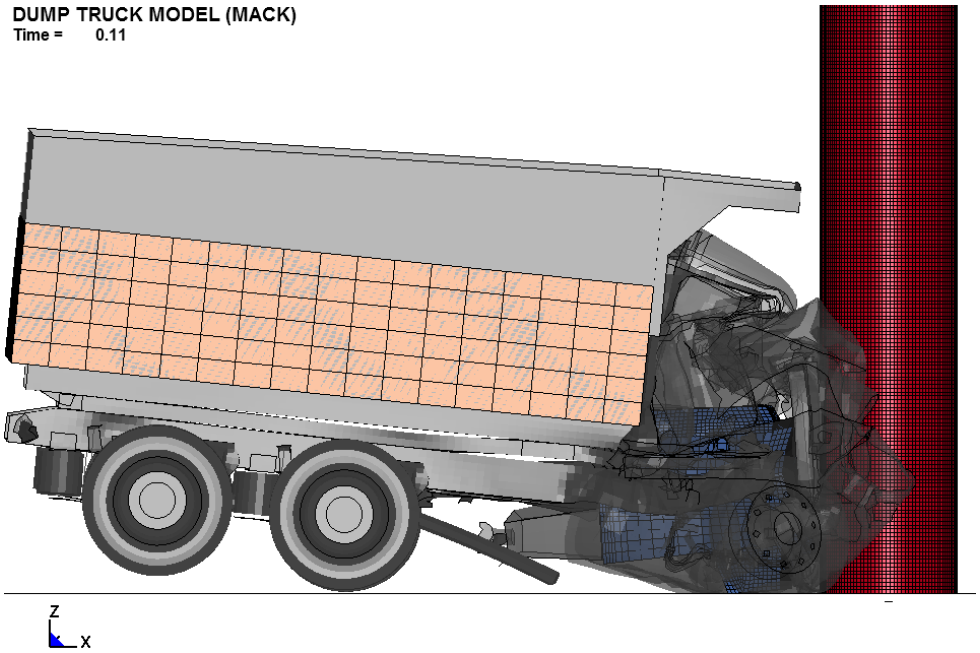

Figure 3.4: TTI dump truck impacting rigid column [2]

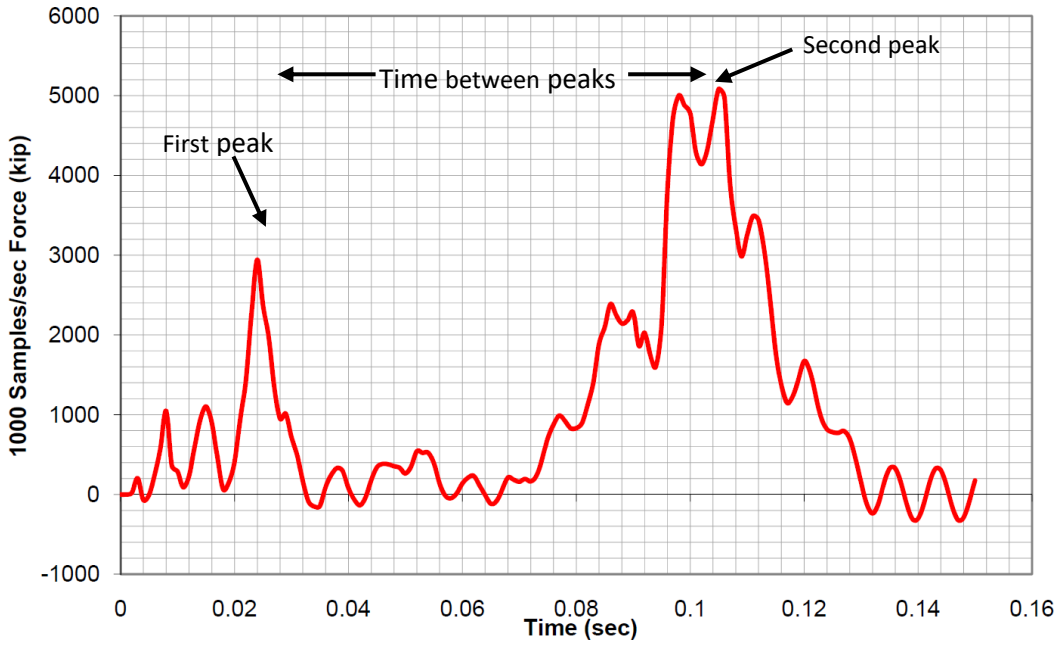

Figure 3.5: Force-Time curve generated by TTI in dump truck-pier collision [2]

The dump truck used by Buth weighs 65 kips so the f800 model used in this study was modified to match by changing the density of the ballast payload. Additionally, the use of a fully rigid column caused early terminations of the f800 model as excessive element failure occurred, so a steel like material was used with the elastic modulus increased to 250 GPa compared to a typical value of 200-210 GPa. This semi-rigid column allows the simulation to run past the second peak and into the time period in which the truck has rebounded off of the column (Figure3.6). A column diameter of 36 inches was selected as it is a typical diameter used by KDOT and an initial velocity of 50 mph is used because it was determined that 50 mph is used more often than 40 mph or 60 mph in other research. Due to the variation in geometry and structure of the two vehicles, the force-time functions initially had somewhat significant differences in the 3 characteristics discussed above. By removing mass from the ballast and adding it to the engine, the force time functions compare reasonably as shown in Figure 3.7. While the magnitude of the first peak for the f800 is only approximately half that of the dump truck and the time between peaks is longer for the f800, the magnitude of the second peak matches closely between the TTI model and the

f800 used for this study. As it is the critical component of the impact, matching the magnitude of the second peak held the highest concern for verifying the behavior of the f800 model. It is suspected that the variation in magnitude of the first peak comes from a larger engine in the TTI dump truck. The difference in time between peaks is likely due to the rigid component directly above the cab on the TTI model causing the ballast to effectively impact the column sooner. For the purposes of this study, the comparison adequately verifies the behavior of the f800.

Figure 3.6: F800 and semi-rigid column at 0.174 seconds after impact

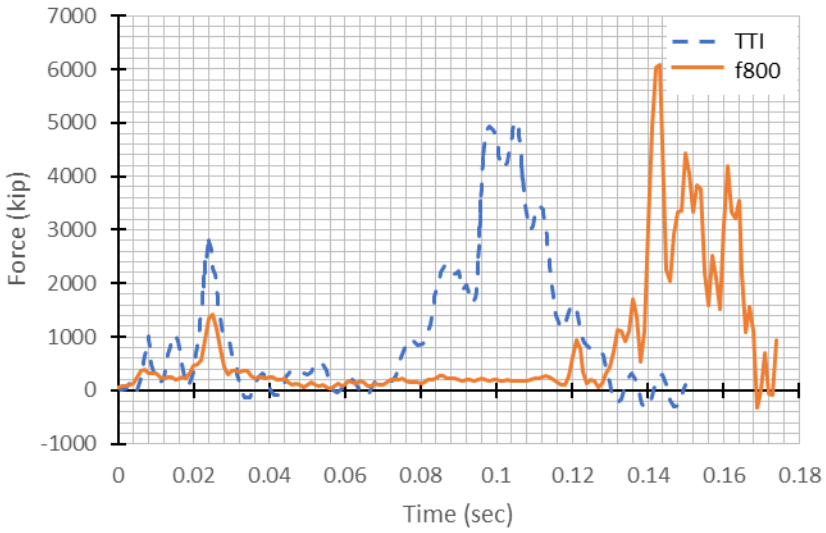

Figure 3.7: Comparison of force-time curves for TTI dump truck and f800

Section 3.2: Column Impact Tests

In addition to the highly rigid column discussed above, impact simulations are also completed with a truly rigid wall and a 36 inch reinforced concrete column. The reinforcement for the RC column, provided by KDOT as a typical design, consists of 13 #8 bars and a #3 spiral cage with 2" clear cover (Figure 3.8). As specified by the KDOT design, the column has a total height of approximately 17' 6". Both ends of the column are fixed for this simulation. While more accurate for the bottom end of the column, the top end of a real column would be less stiff and depend on the bridge superstructure. Fixing both ends, however, keeps the column more comparable with the other simulations. The results of this simulation shown in Figures 3.9 and 3.10 demonstrate that the concrete column completely fails in the impact scenario. Figure 3.9 reveals that the column has completely failed before the primary payload ballast has even contacted the column. This behavior is also reflected in the force-time curve in Figure 3.11. A small first peak can be observed, reaching only 260 kips, at the beginning of the impact and quickly dissipates as the column fails to resist further load, so a second peak never develops.

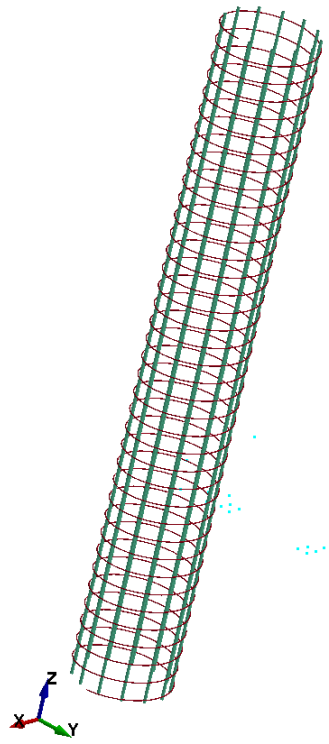

Figure 3.8: RC column rebar design as provided by KDOT

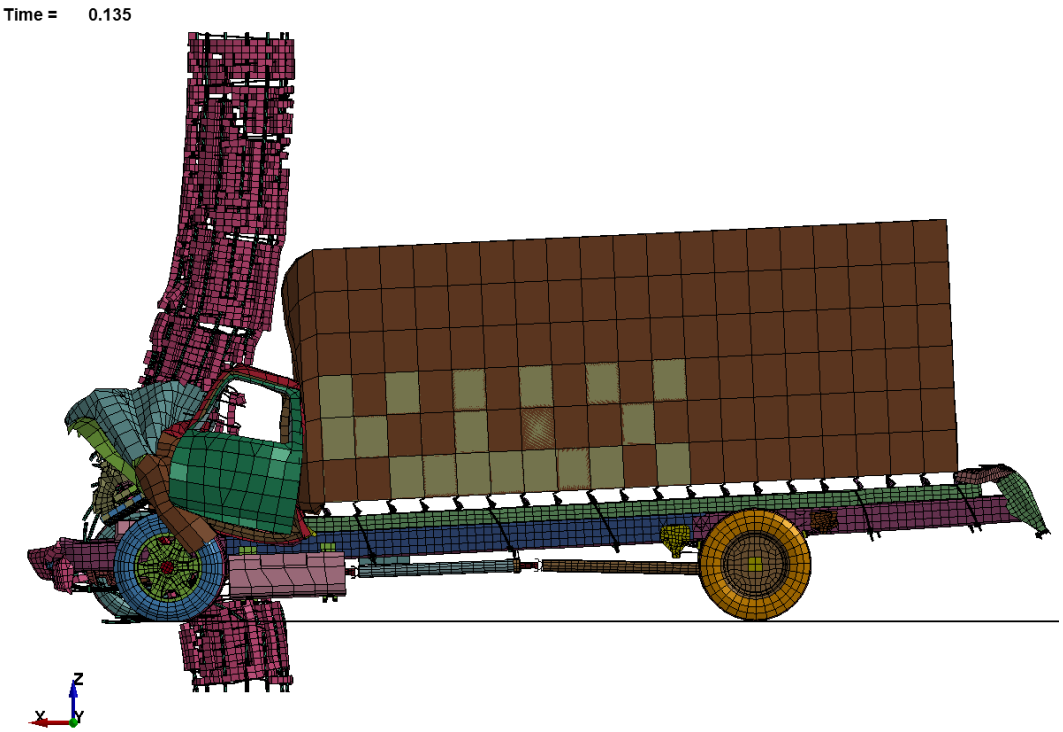

Figure 3.9: F800 and KDOT RC column at t=0.135 seconds

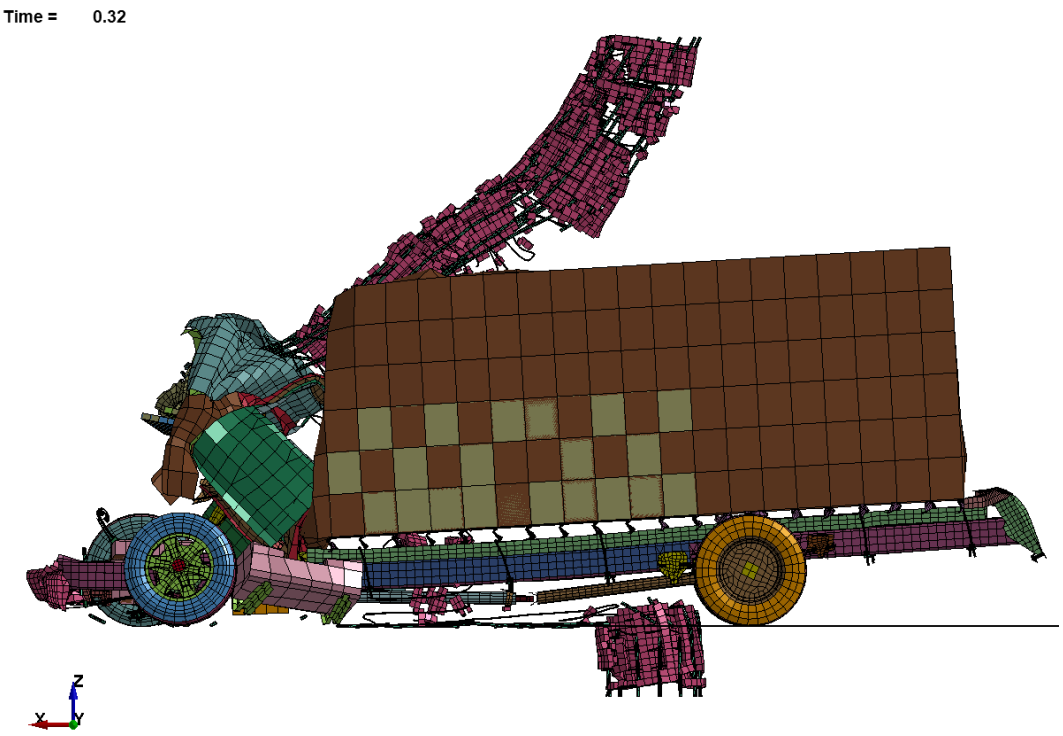

Figure 3.10: F800 impacting KDOT RC column at t=0.32 seconds

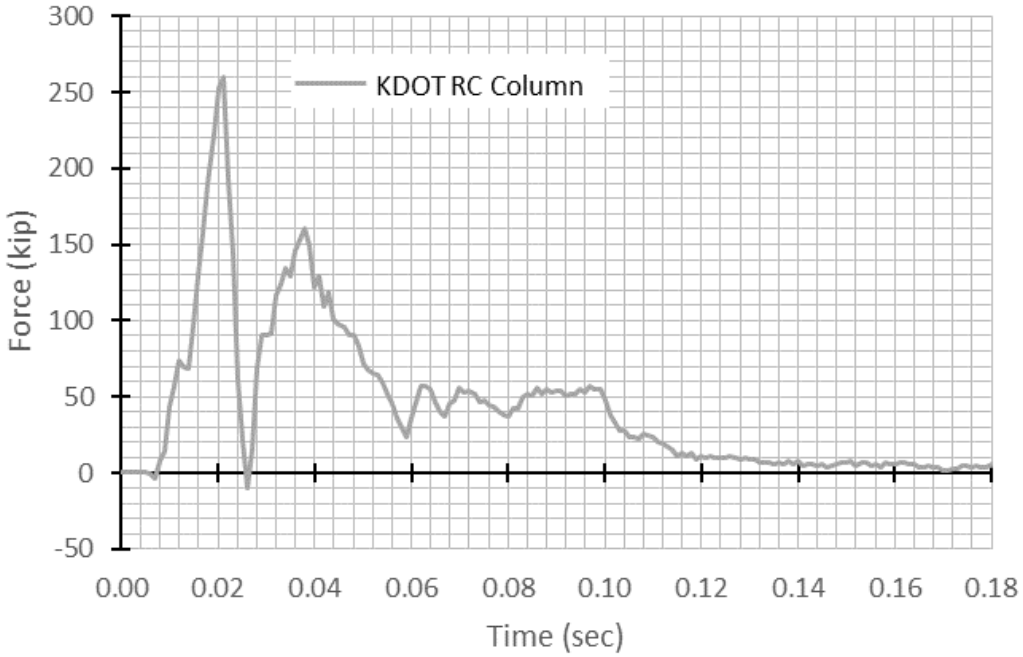

Figure 3.11: Force-time curve for f800 impacting KDOT RC column

As demonstrated in Figures 3.11 and 3.7, the properties of the column drastically affect the magnitudes and time characteristics of the force-time curve. With the goal of capturing the full possible force throughout an impact scenario, a simulation was performed with a fully rigid plane. Due to the high mass of the ballast, the model terminates as elements experience negative volume when the ballast crushes the cab section (Figures 3.12 and 3.13). The curve shown in Figure 3.14 shows the extremely high reaction forces for the rigid wall as the ballast begins to transfer its energy through the impact.

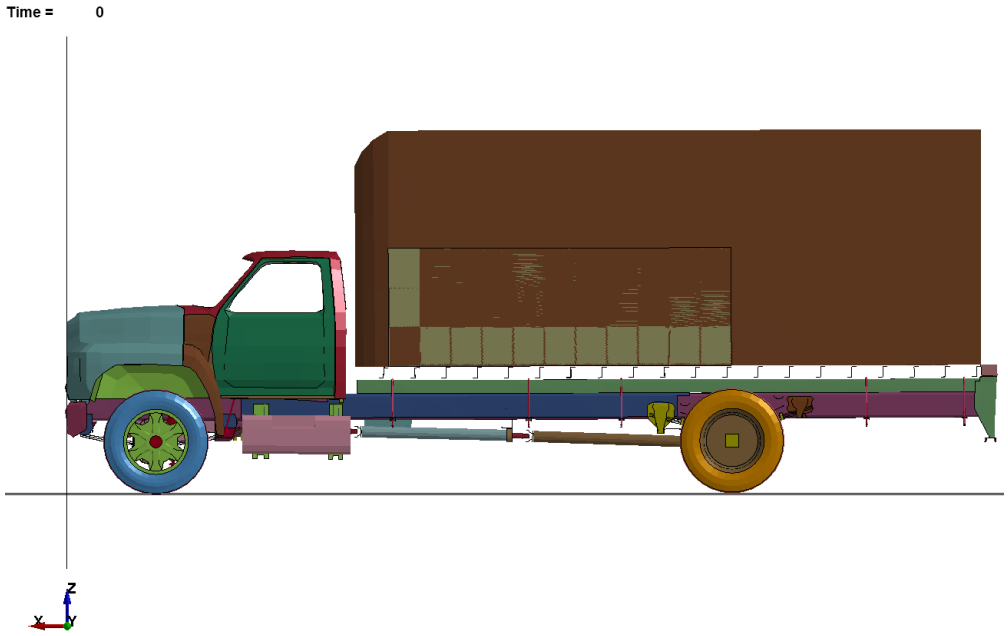

Figure 3.12: Initial f800 impact on rigid wall

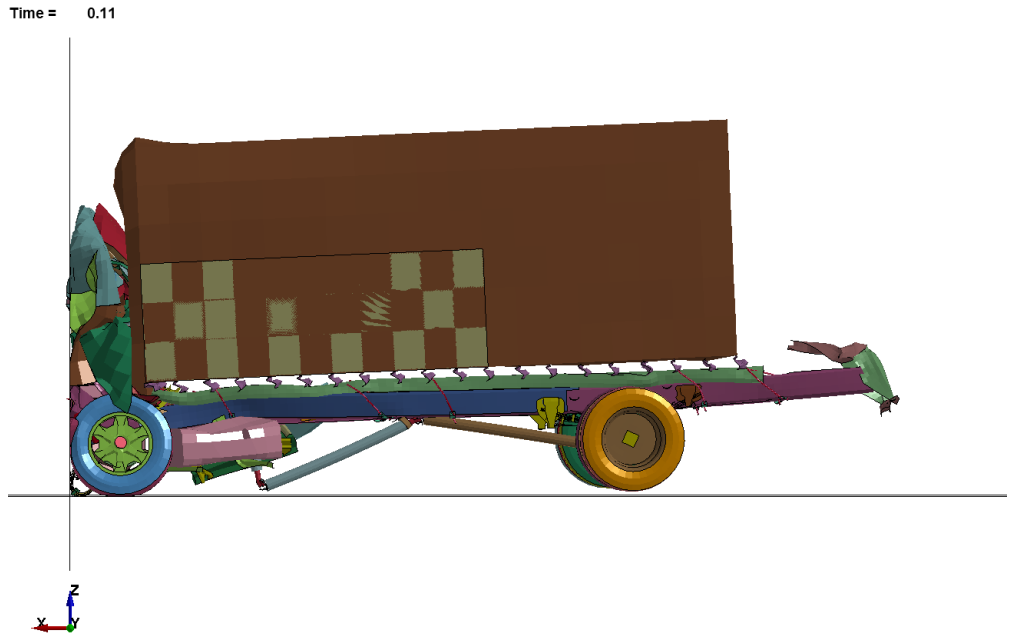

Figure 3.13: Final state of f800 impact on rigid wall

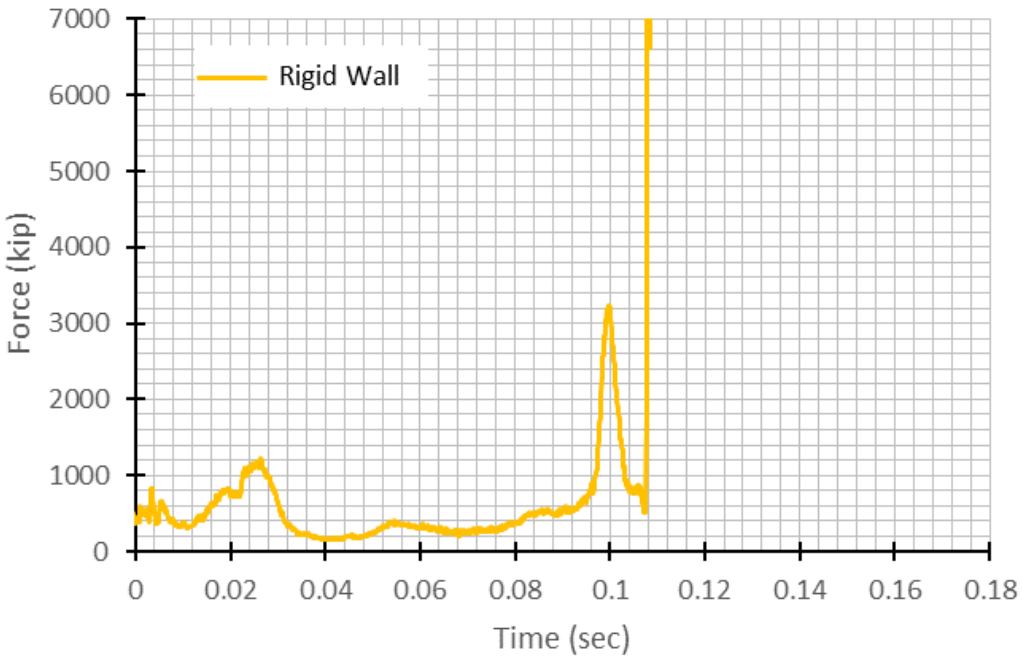

Figure 3.14: Force-time curve for f800 impacting rigid wall

Figure 3.15 combines the data from all three tests discussed above: the semi-rigid column, the KDOT RC column, and the fully rigid wall. As mentioned previously, the magnitude of the two peaks and the time between peaks are significant. The comparison demonstrates significant variation in all three characteristics as the column parameters are changed. The TTI report that functions as a basis for the AASHTO recommendation of 600 kips used a steel pipe column filled with concrete. It can be assumed that the column used is much stiffer than a typical reinforced concrete bridge pier. This suggests the recommendation of 600 kips may be significantly conservative even without considerations for protective barriers.

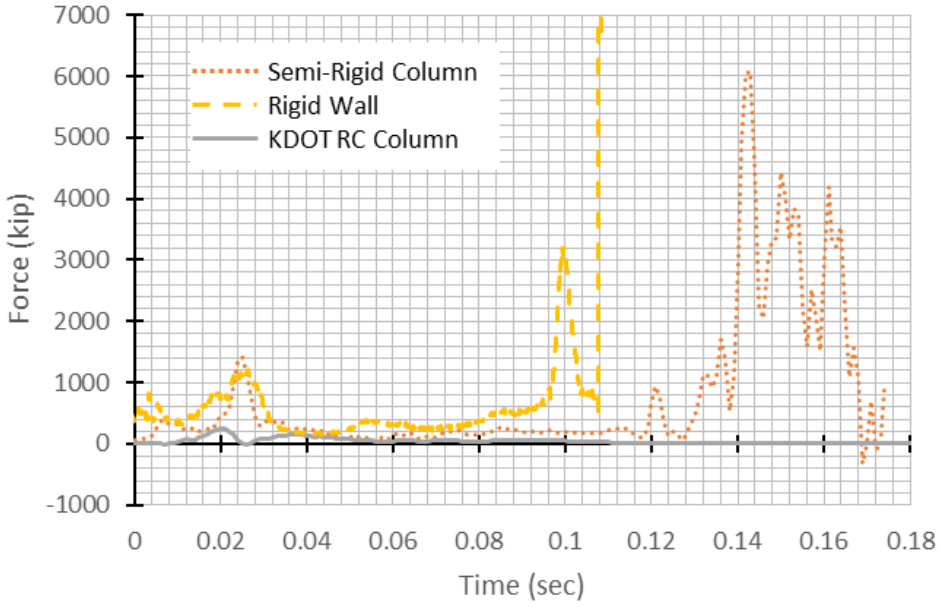

Figure 3.15: Comparison of semi-rigid column, rigid wall, and KDOT RC column force-time curves

Section 3.3: Barrier Impact Tests

The full barrier simulation used in this study are designed according to the KDOT design in Figure 1.1 and extended for 65 feet as shown in Figures 3.16 and 3.17. The Simplified Johnson Cook material model (LS-DYNA MAT_098) [16] was selected for the steel rebar. Material testing and calibration of material models was beyond the scope of this study, so material parameters for HRB400 grade steel are used as

determined by Lin [17], giving a yield strength of 58 ksi for the rebar. Additionally, steel density was defined as 489 pcf and Young's Modulus as 30,000 ksi with Poisson's Ratio as 0.3. The Karagozian & Case Concrete Model – Release 3 material model (LS-DYNA MAT_072R3) was selected for the concrete material model. Material parameters provided for MAT_072R3 in the user's manual [16] were used for this study. These properties include a compressive strength of 6500 psi, and a density of 152 pcf. More accurate parameters can be obtained via laboratory testing of the concrete used and calibration from that data. All rebar is modeled as beam elements and the barrier as solid elements. The reinforcement is constrained within the concrete barrier using a Lagrange-in-Solid constraint.

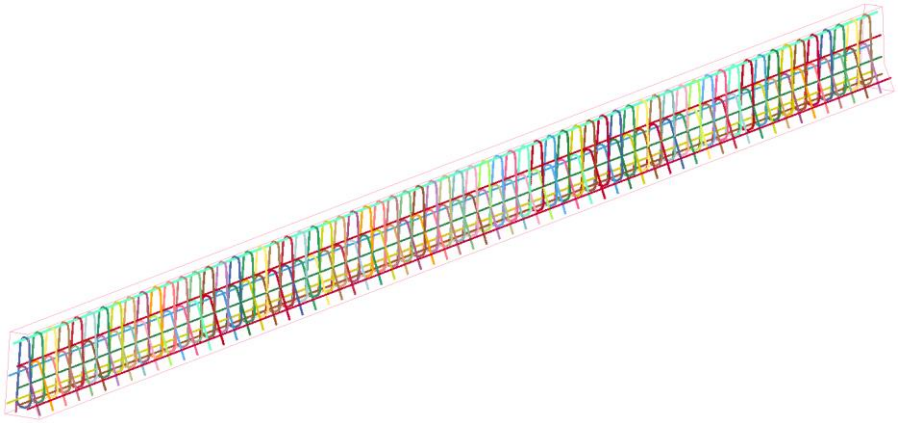

Figure 3.16: Reinforcement as modeled for transient dynamic simulations

Figure 3.17: Concrete barrier mesh as modeled for transient dynamic simulations

In this study, 20 FEA simulations are completed for barrier impacts using the f800 model previously discussed. Initial vehicle velocity, angle of impact and boundary conditions of the barrier all vary to create a range of scenarios. In every simulation, the ends of the barrier are completely fixed. The bottom ends of the stirrups at every 12 inches (Figure 3.18) are either fixed or free to create an envelope bounding the actual condition of rebar extending into the pavement. Fixing the rebar creates a more rigid condition as it requires the rebar to fail rather than allowing it to pull out of the base pavement. Initial velocity is either 40 mph or 50 mph and angle of impact includes 15°, 25°, 35°, 45°, and 90° as defined Figure 3.19.

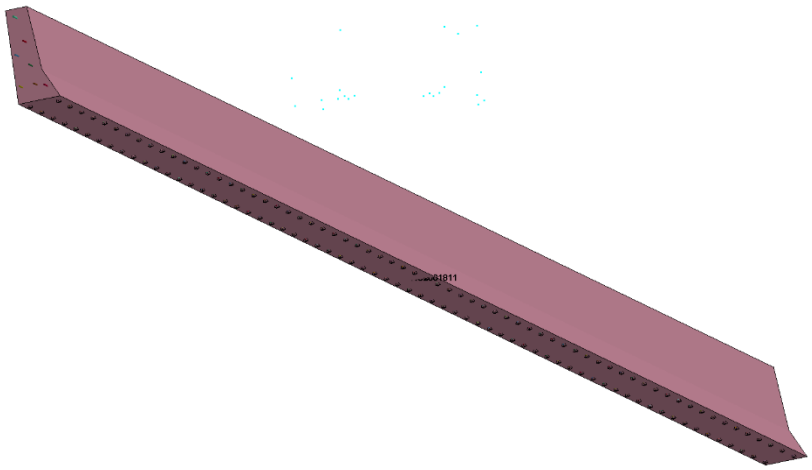

Figure 3.18: Fixed ends of rebar against pavement

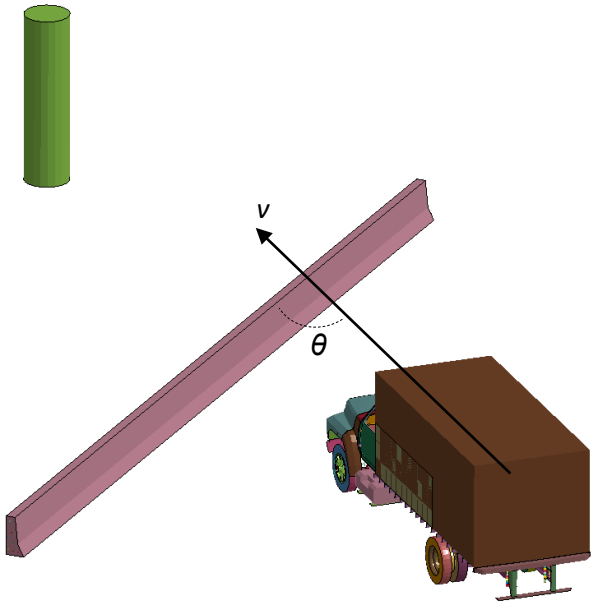

Figure 3.19: Representation of initial velocity, *v*, and angle of impact, θ

Before extracting any numerical data, visual inspection demonstrates a significant difference between the fixed and free boundary conditions as well as the extreme angles of approach, 15° and 90°. While the lack of fixity allows the barrier to slide, the lower angle also redirects the truck away from the initial trajectory and along the barrier instead (Figure 3.20). The fixed bottom and 90° approach, however, allows the truck to punch directly through the barrier in short time without affecting the trajectory or absorbing as much energy (Figure 3.21). While 90° is clearly the critical case, the likelihood of a truck impacting the barrier at such a steep angle while also in a position to strike a bridge pier is extremely low. Additionally, the 600 kip force in AASHTO also corresponds to a 15° approach [1]. This visual inspection shows promising results for a justification to reduce the required design force.

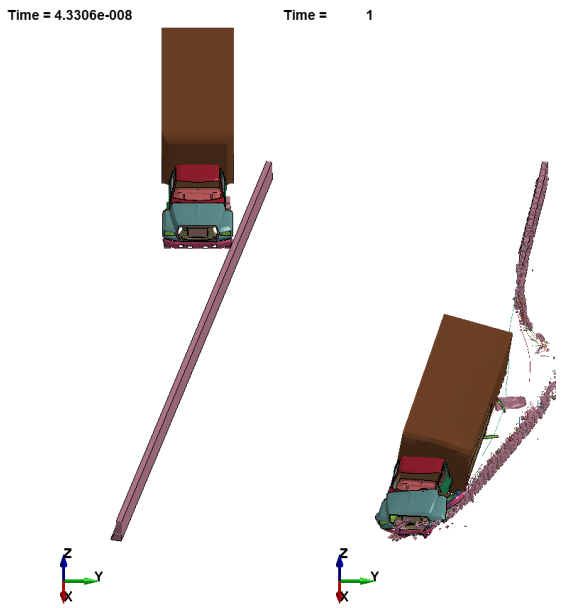

Figure 3.20: Free barrier at 15°; t=0 & t=1 seconds

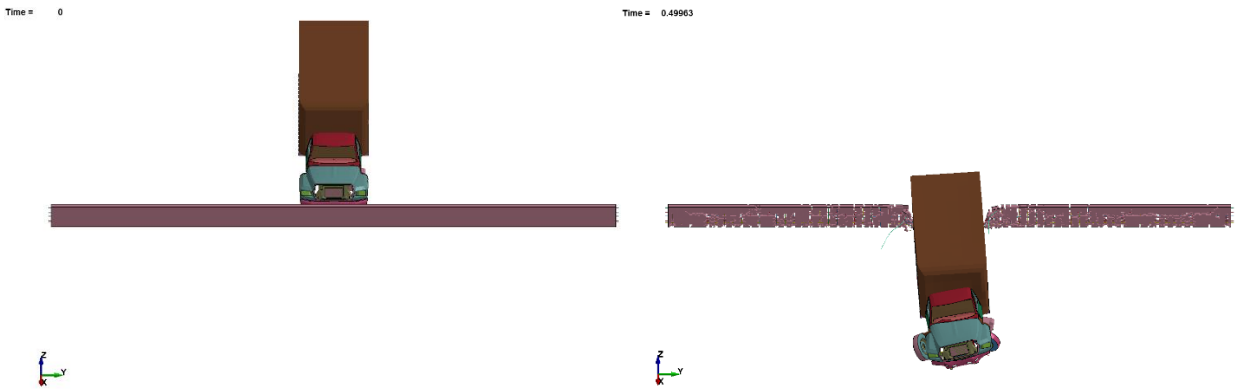

Figure 3.21: Fixed barrier at 90; t=0 and t=0.5 seconds

Three parameters of the truck will be tracked and discussed in the results for the 20 barrier impact scenarios: velocity, kinetic energy, and internal energy. While velocity and kinetic energy relate more directly to the potential pier damage, inclusion of the internal energy provides a more complete understanding of the energy transfer throughout the collision. All simulations have been adjusted so that zero seconds is the moment of impact and the curves end where the simulation either terminates

or the truck has passed the influence of the barrier. For each parameter, four graphs are created resulting in a total of 12 to summarize the data. Each combination of initial velocity, 40 mph or 50 mph, and barrier boundary conditions, fixed or free, are shown in a graph including each angle of approach.

Velocity change is the simplest way to analyze the contribution of the barrier, but perhaps the least useful. The curves (Figure 3.22) show a consistent trend where 90° is the least affected. As mentioned previously, the high angle offers little resistance to the truck. The steeper angles, however, have a better chance to reduce the velocity as the truck has to pass through a longer section of the barrier. In the extreme cases, the truck may even be redirected back towards the road. This explains the similarity between 15° and 25°. In the 15° scenario, the truck is redirected towards the road so the velocity can be maintained over the longer distance. In the 25° scenario, however, the truck is not redirected and instead has to continuously plow through the barrier, but for a slightly shorter time. The data shows the two conditions have similar trendlines in every scenario.

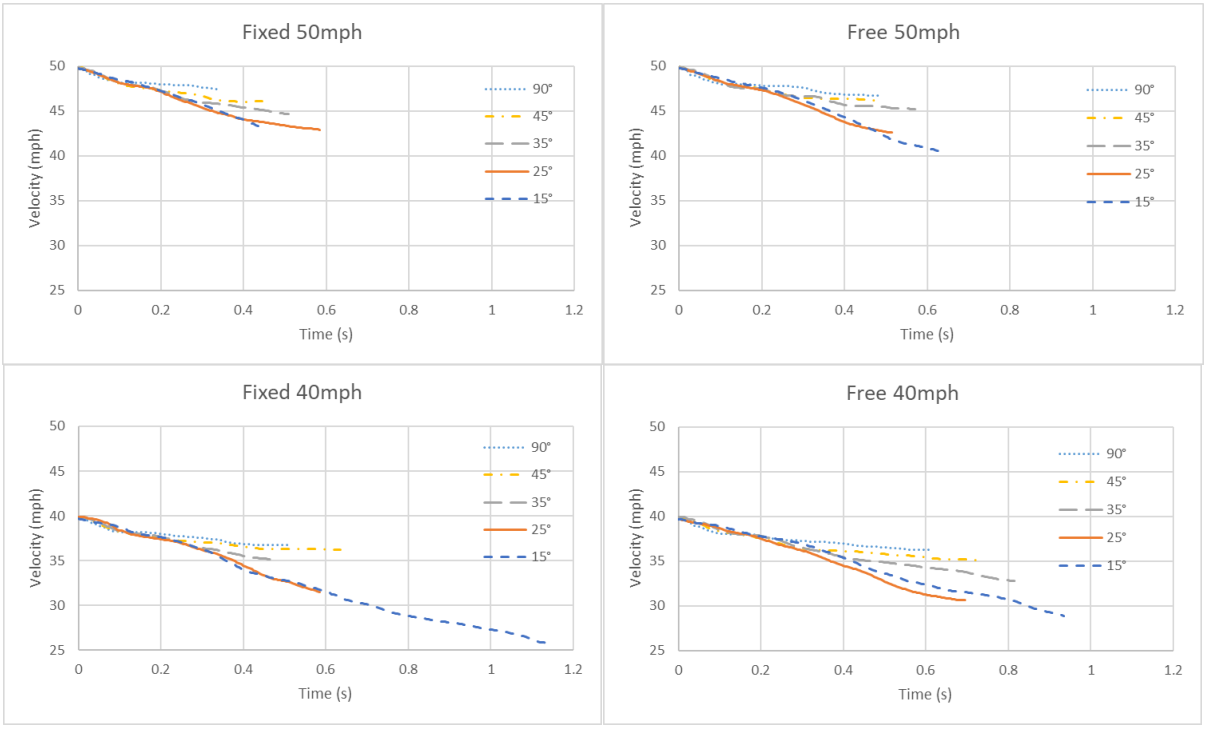

Figure 3.22: Velocity histories for all 20 barrier simulations

The next measured property for the truck is kinetic energy. The results follow the velocity change exactly (Figure 3.23). As seen in both Figures 3.22 and 3.23, it takes between 0.16 seconds and 0.2 seconds for the curves to diverge depending on the angle of approach. This time can be correlated to approximately the time until the first contacted wheel rotates to match the direction of the barrier. The rotation of the tire allows the velocity and energy to be gently redirected before the inertia of the vehicle and payload carry the truck along the original angle of approach.

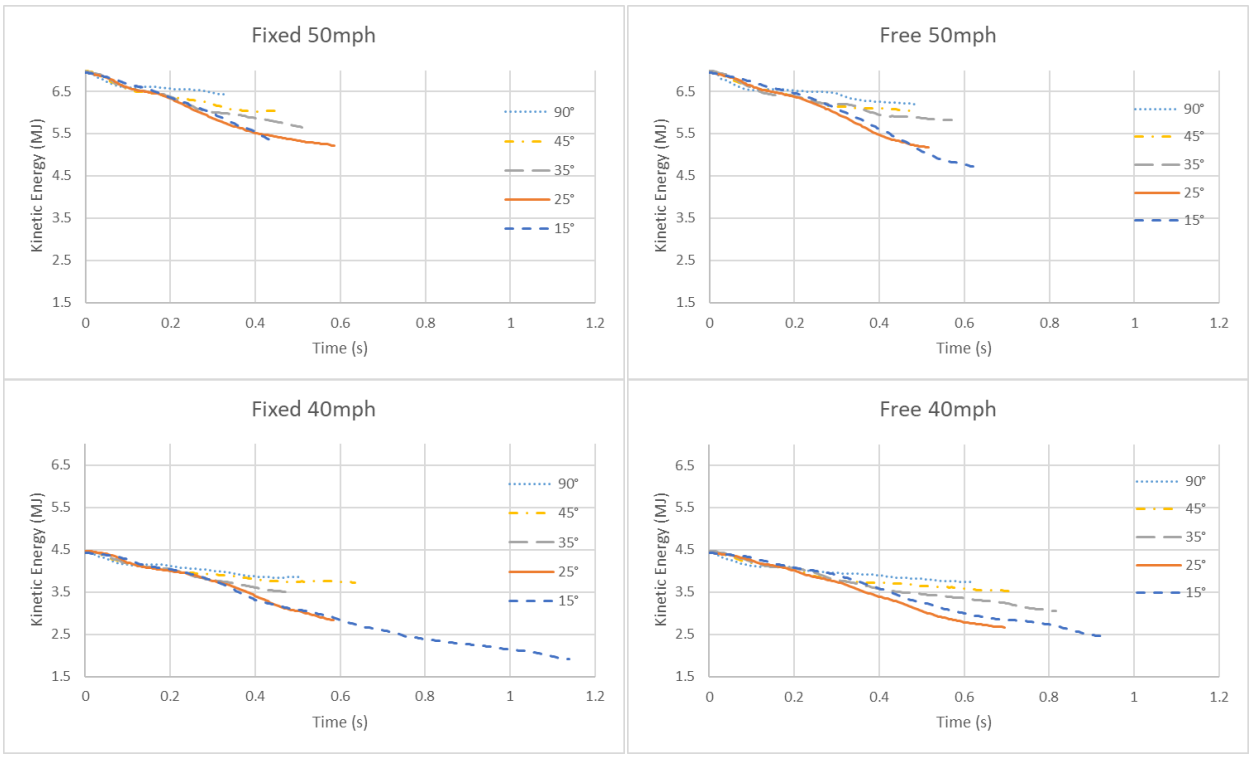

Figure 3.23: Kinetic Energy histories for all 20 barrier simulations

Internal energy of the truck is another important result when understanding the full scenario. For this purpose, it represents the damage inflicted on the truck. The 90° approach has the highest initial change in internal energy as the truck slams into the perpendicular barrier. The truck has no opportunity to dissipate energy through redirection and experiences high damage. However, as the entire truck passes

through the same narrow region, a smaller amount of the barrier needs to be destroyed so the rate of change of internal energy slows quickly. For the lower angles such as 15° and 25°, the truck initially changes directions and experiences low damage. As it penetrates the barrier it then needs to continuously push through the barrier and experiences a high amount of damage and passes the internal energy of the 90° approach.

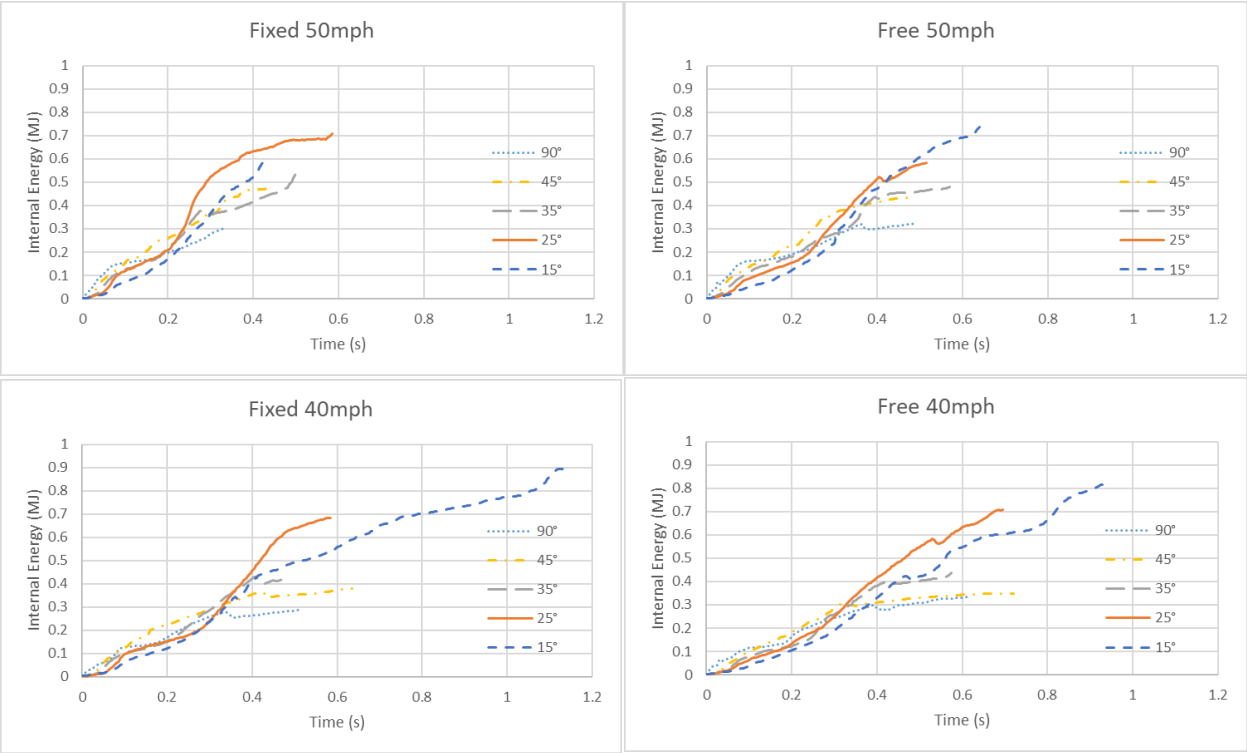

Figure 3.24: Internal Energy histories for all 20 barrier simulations

Table 3.1 summarizes the changes of energy and velocity during the simulations. While the percent changes in kinetic energy and velocity offer more context for the effectiveness of the barrier in these simulations, the percent can vary significantly with the vehicle in question. For this reason, the magnitudes of change are more universal when considering other vehicles and comparing to other studies. The most important results of this study are the change in kinetic energy and velocity. The

change in kinetic energy is the most appropriate value to consider when considering the change in the impact force on a column after traversing the barrier. The percent change in kinetic energy ranges from a minimum of 8% to a maximum of 57%. It is important to note that the lower bound occurs in the case of a 90° approach and is highly unlikely. The 57% reduction, however, occurs for a 15° approach as is the basis for the design specifications. The simplest analysis of this data suggests it might be appropriate to reduce the 600 kip design force by 57% as well. This reduction would have a significant impact on the adequacy of existing columns. Further research is required to determine how the reduction in kinetic energy may affect the required design force.

Table 3.1: Summary of LS-Dyna simulation results

Boundary Condition	Initial Velocity	Approach Angle	Magnitudes of Change			Percent Changes	
			KE (MJ)	IE (MJ)	V (mph)	KE	Velocity
Fixed	40 mph	15°	2.52	0.89	13.9	57%	35%
		25°	1.64	0.68	8.4	37%	21%
		35°	0.98	0.42	4.9	22%	12%
		45°	0.74	0.38	3.7	17%	9%
		90°	0.62	0.29	3.1	14%	8%
	50 mph	15°	1.60	0.61	6.4	23%	13%
		25°	1.73	0.71	6.8	25%	14%
		35°	1.33	0.56	5.2	19%	11%
		45°	0.95	0.47	3.8	14%	8%
		90°	0.57	0.31	2.4	8%	5%
Free	40 mph	15°	2.01	0.82	10.8	45%	27%
		25°	1.76	0.71	9.1	40%	23%
		35°	1.42	0.44	7.1	32%	18%
		45°	0.94	0.35	4.7	21%	12%
		90°	0.72	0.33	3.7	16%	9%
	50 mph	15°	2.29	0.73	9.4	33%	19%
		25°	1.78	0.58	7.2	26%	14%
		35°	1.16	0.48	4.7	17%	9%
		45°	0.94	0.44	3.8	14%	8%
		90°	0.78	0.32	3.2	11%	6%

Chapter 4: Yield Line and Static FEA

Section 4.1: Yield Line Analysis

Section 13: Railings of the AASHTO LRFD Bridge Design Specification provides a process for using yield line analysis to determine the capacity of concrete parapets and barriers to resist transverse loads. Yield line analysis functions on the basis of balancing external work from an applied load and internal work as the material fails and an assumed yield line forms. Unfortunately, the guidelines are intended for cross-sections with straight sides and evenly distributed reinforcement in addition to a rectangular beam component along the top as shown in Figure 4.1. Additionally, the design specification provides Table 4.1 which provides values that are allowed to be used depending on the crash test level rating of the barrier. Due to the difference in geometry, this study uses the values of length in table 4.1 as a guide in a new set of yield line analysis calculations following the same failure pattern shown in Figure 4.1.

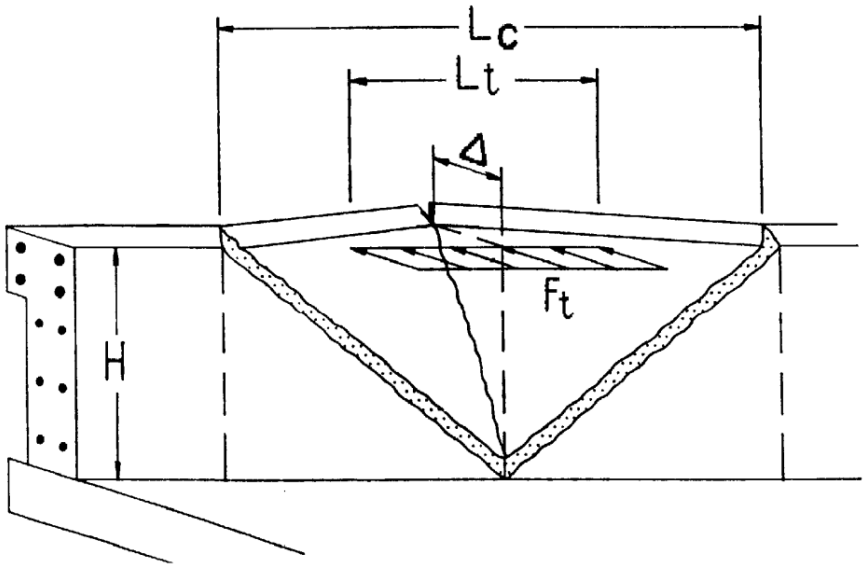

Figure 4.1: Concrete barrier yield line pattern [1]

Table 4.1: Allowable design values for railings [1]

Design Forces and Designations	Railing Test Levels					
	TL-1	TL-2	TL-3	TL-4	TL-5	TL-6
F_t Transverse (kips)	13.5	27.0	54.0	54.0	124.0	175.0
F_L Longitudinal (kips)	4.5	9.0	18.0	18.0	41.0	58.0
F_v Vertical (kips) Down	4.5	4.5	4.5	18.0	80.0	80.0
L_t and L_L (ft)	4.0	4.0	4.0	3.5	8.0	8.0
L_v (ft)	18.0	18.0	18.0	18.0	40.0	40.0
H_e (min) (in.)	18.0	20.0	24.0	32.0	42.0	56.0
Minimum *H* Height of Rail (in.)	27.0	27.0	27.0	32.0	42.0	90.0

Using a value of Lt=42” for a TL-4 railing, the external work from an applied distributed force, Ft, can be defined as

$$U_{external} = 42" \, F_t \, (1 - \frac{10.5}{32 \tan\propto}) \qquad \text{Equation 4.1}$$

where $\propto$ is the angle between the vertical axis and the yield line as defined in Figure 4.2.

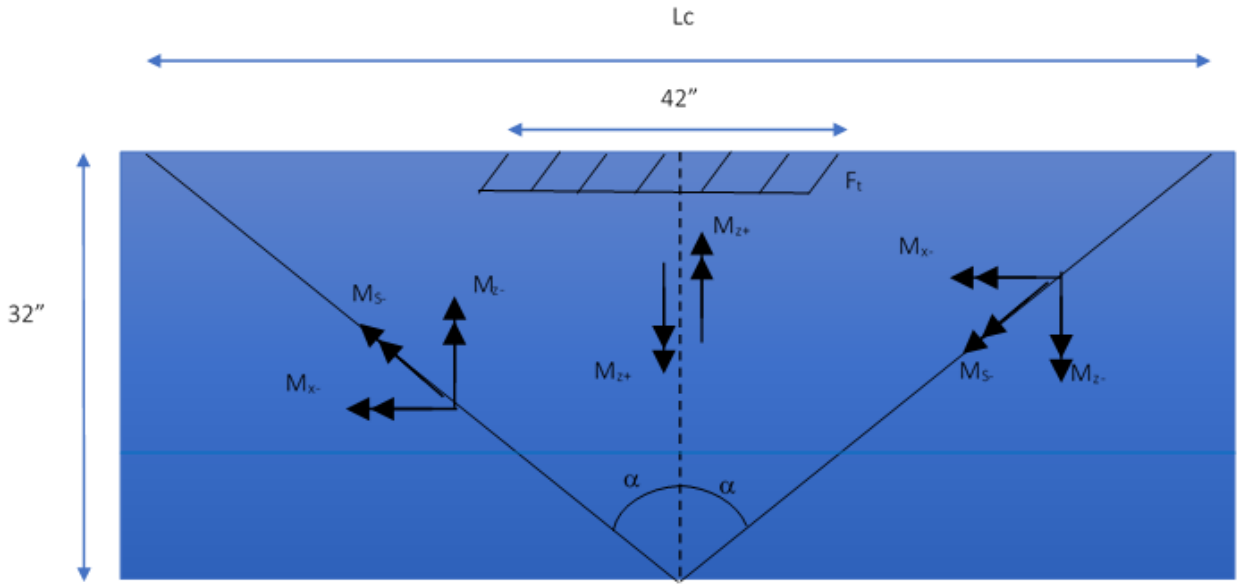

Figure 4.2: Format of yield line and definition of terms

Following the yield line above, the deformation, Δ, will occur at the center of the applied load F_t. Figure 4.3 shows simple representations of how the barrier deforms linearly between the yield lines and the top center point of the barrier.

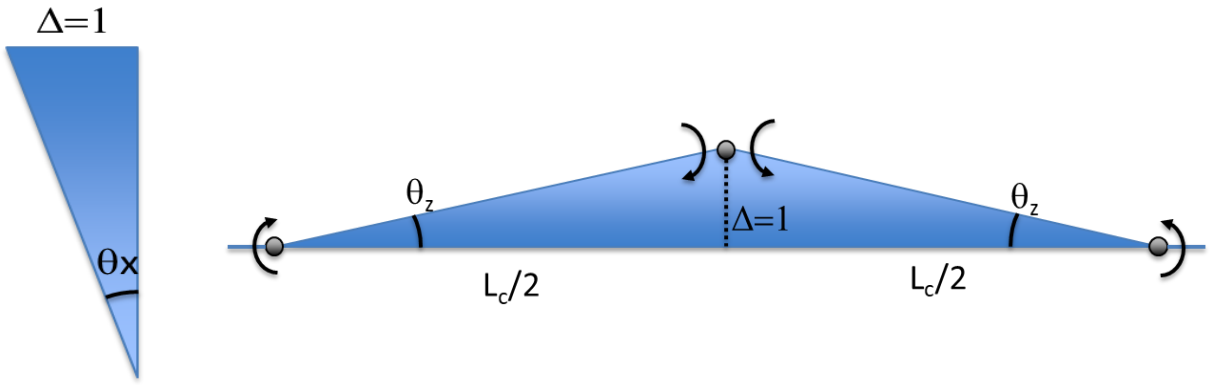

Figure 4.3: Side (left) and top (right) views of ideally deformed barrier

Yield line analysis requires the moment capacity along each yield line when calculating the internal work. For the KDOT barrier, moments around the x and z axes as established in Figure 4.4 are needed.

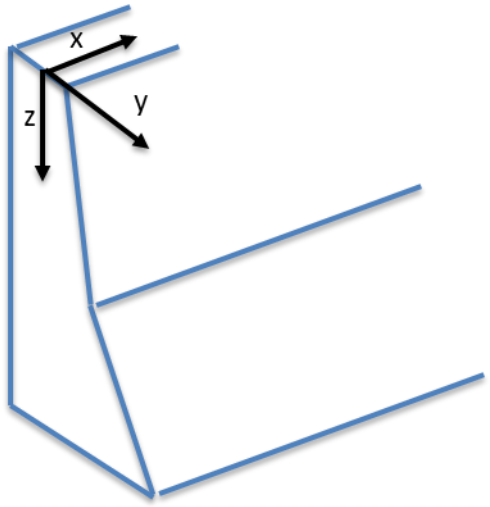

Figure 4.4: Definition of yield line coordinate system

Due to the changing thickness of the barrier as heights changes and the nonuniform distribution of reinforcement, approximate Equations for Mx and Mz were developed as a function of height, z. A weighted average was used to create an effective depth of reinforcement and reinforcement per inch throughout the height of the barrier. With the barrier being split at z=22" (Figure 4.5), piecewise functions for Mz (Equations 4.2 - 4.5) were created for both positive and negative bending. Similar Equations (Equations 4.6 & 4.7) were developed for Mx, but only in the negative direction. Bending at the center of the yield line formation is considered positive moment while bending of the diagonal yield lines is considered negative for both axes, z and x. Because the effective depth of reinforcement is averaged independently over z and z', the value for M_{z+} at z=22" does not match the value for $M_{z'+}$ at z'=0". This is apparent as d_2 does not equal d'_2. The same applies for M_{z-} and $M_{z'-}$.

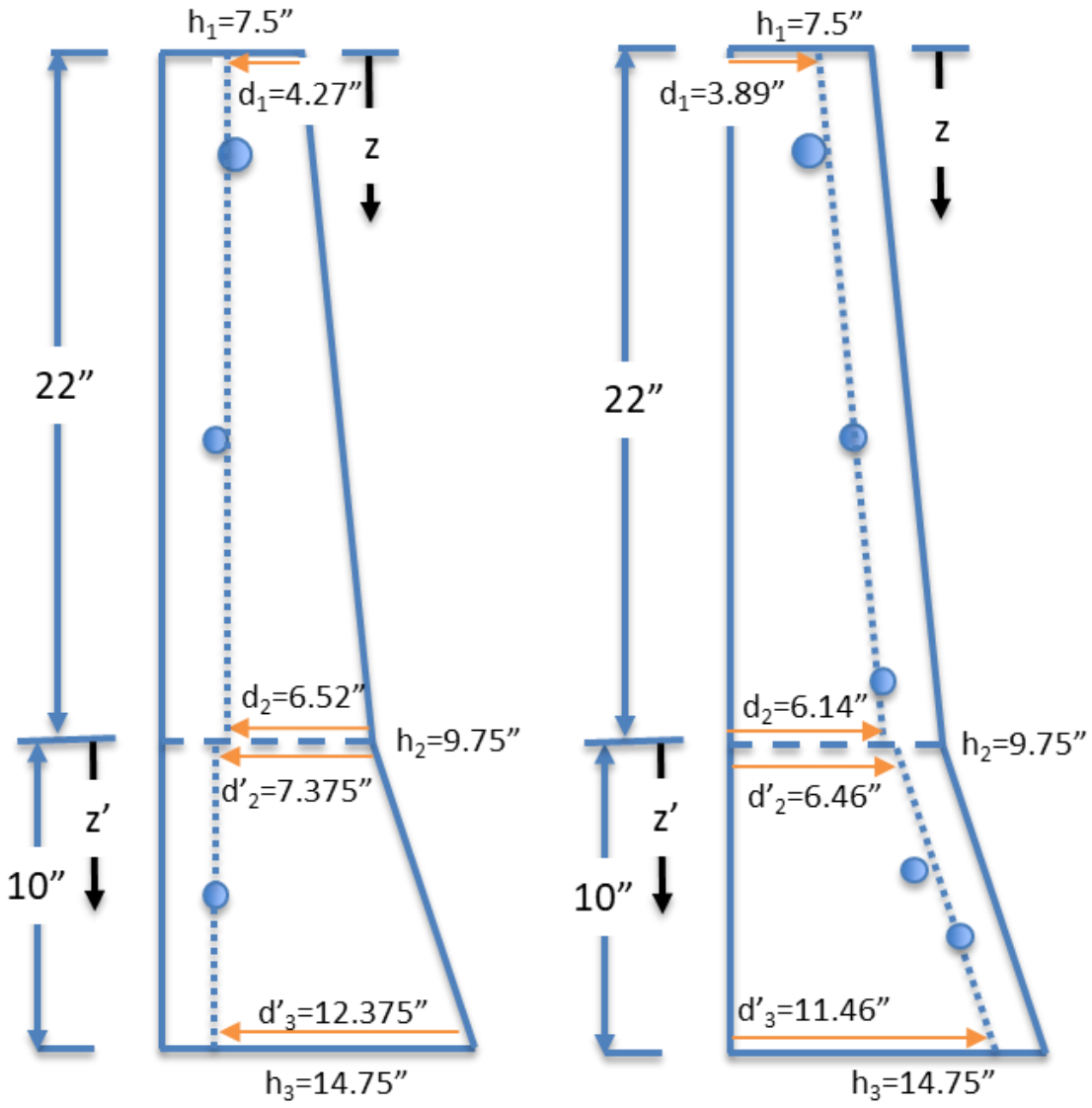

Figure 4.5: Rebar diagrams for z-axis positive (left) and negative (right) moments

$$M_{z+} = 6.98\frac{kip-in}{in} + 0.178z\frac{kip-in}{in} \quad \text{Equation 4.2}$$

$$M_{z'+} = 8.64\frac{kip-in}{in} + 0.6z'\frac{kip-in}{in} \quad \text{Equation 4.3}$$

$$M_{z-} = 8.13\frac{kip-in}{in} + 0.234z\frac{kip-in}{in} \quad \text{Equation 4.4}$$

$$M_{z'-} = 14.66\frac{kip-in}{in} + 1.2z'\frac{kip-in}{in} \quad \text{Equation 4.5}$$

Idealized cross-section cuts were made at z=0, z=22 and z=32 as shown in Figure 4.6. Using these cuts, the moment capacity M_{x-} was calculated at each location and a piecewise function created to interpolate the moment as a function of the height z (Equations 4.6-4.7).

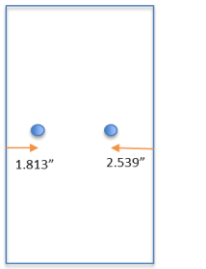

$$z = 0"$$
$$M_{x-} = 7.336\,\frac{k-in}{in}$$

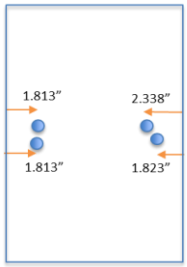

$$z = 22"$$
$$M_{x-} = 22.362\,\frac{k-in}{in}$$

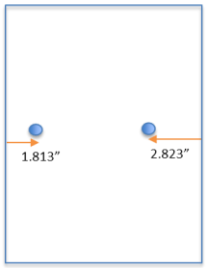

$$z = 32"$$
$$M_{x-} = 18.134\,\frac{k-in}{in}$$

Figure 4.6: XY-plane cross-sections of KDOT Barrier

$$M_x = 7.34\frac{kip-in}{in} + 0.683z\frac{kip-in}{in} \qquad \text{Equation 4.6}$$

$$M_{x'} = 22.36\frac{kip-in}{in} + 0.423z'\frac{kip-in}{in} \qquad \text{Equation 4.7}$$

Figure 4.7 provides a visual representation of the relationship between M_x and z. It can be seen that the maximum moment capacity is located at the overlap of the two stirrups. As maximum moment will likely occur at the base of the barrier, this suggests there may be potential for optimization of the design.

Similarly, the capacities for negative bending around the z-axis are larger than the positive direction. With traffic impacts causing positive z-axis bending in the barrier, there may be potential for improvement in both axes.

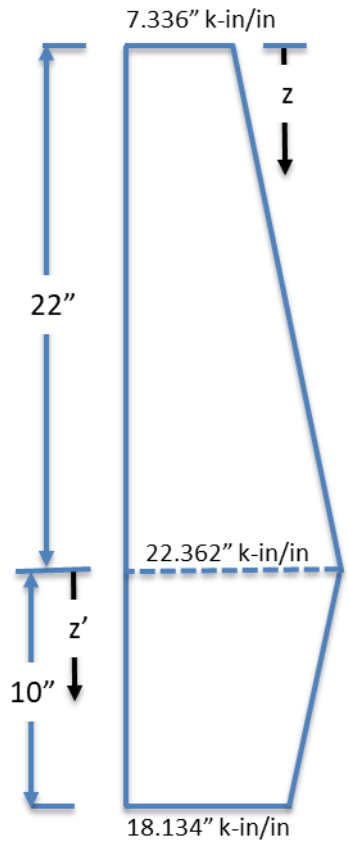

Figure 4.7: Representation of M_x as a function of z

Following Figure 4.2, the complete internal energy is given below in Equation 4.8. The first two terms are caused by the center, vertical yield line. The last term, M_{S-}, follows the diagonal yield line in negative bending, as a function along the diagonal yield line, and can be decomposed into the x-axis and z-axis components as introduced above (Figure 4.2). After completing the required substitutions and integrations, a simplified Equation for the internal energy (Equation 4.10) develops as a function of only the angle, $\propto$.

$$U_{internal} = \int_0^{22} M_{z+}(z)\ 2\theta(z)\ dz + \int_0^{10} M_{z'+}(z')\ 2\theta(z')\ dz + 2\int M_{S-}(S)\ \theta(S)\ ds\ )$$

Equation 4.8

$$ds = \sqrt{dx^2 + dz^2} = dz\sqrt{1 + (\tan \propto)^2}$$ Equation 4.9

$$U_{internal} = 19.556 \cot \propto + 33.072 \sec \propto + 27.639 \csc \propto$$ Equation 4.10

Combining Equations 4.1 and 4.10 by equating internal and external energy yields Equation 4.11. Minimizing the Equation and solving for Ft, provides the critical load for the barrier and the length Lc over which the yield lines form. In this set of calculations, Ft is found to be 134.8 kips with a length, Lc, of 106.2 inches. The corresponding angle, $\propto$, is $58.9°$.

$$F_t = \frac{19.556 \cos \propto + 33.072 \tan \propto + 27.639}{42 \sin \propto - 13.781 \cos \propto}$$ Equation 4.11

The load provided by AASHTO [1] in table 4.1 suggests a load of only 54 kips for a TL-4 railing, which most closely matches the barrier of concern in this study. While yield line analysis is a work-based approach to finding the critical load, it does not directly give energies. An actual displacement is required for energy and the yield line approach assigns a deformation of Δ=1 for the purpose of solving. Abaqus FEA will be introduced to solve for values of the energy.

Section 4.2: Abaqus Model

In Abaqus, the barrier is modeled using the smeared cracking material model for the concrete [18]. Concrete for this model is defined with a 4000 psi 28-day compressive strength, 475 psi rupture strength and Poisson's ratio of 0.15. The common approximation of $E = 57000\sqrt{f'c}$ [19] is used to calculate a

Young's modulus of 3604997 psi. To verify the material behavior, a 4"x8" cylinder Abaqus model (Figure 4.8) was simulated in compression and tension. The results (Figure 4.9) do not plot the entirety of the expected stress-strain relationships. Non-convergence leads to a partial curve, but the tests still demonstrates that the material is behaving as expected beyond the peak stress. Finer mesh would likely improve the accuracy as demonstrated by Chaudhari [20].

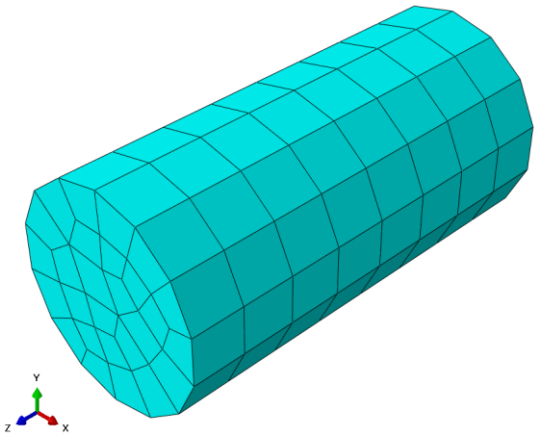

Figure 4.8: 4"x8" concrete cylinder model

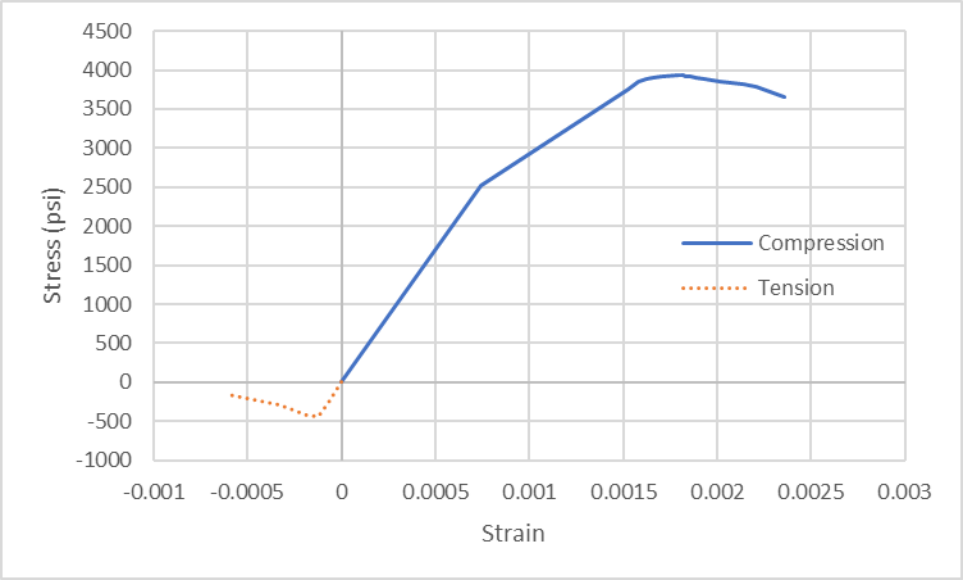

Figure 4.9: Stress-Strain curves generated by cylinder model

All steel rebar was modeled with a much simpler elastic-plastic material model. With an elastic modulus of 29000 ksi and yield strength of 60 ksi, the rebar has a nearly flat plastic plateau, rising only 500 psi over a strain of 0.025.

The full barrier was modeled following the barrier design provided by KDOT (Figure 1.1). The reinforcement was modeled as beam elements constrained in solid elements for the concrete (Figures 4.10 & 4.11).

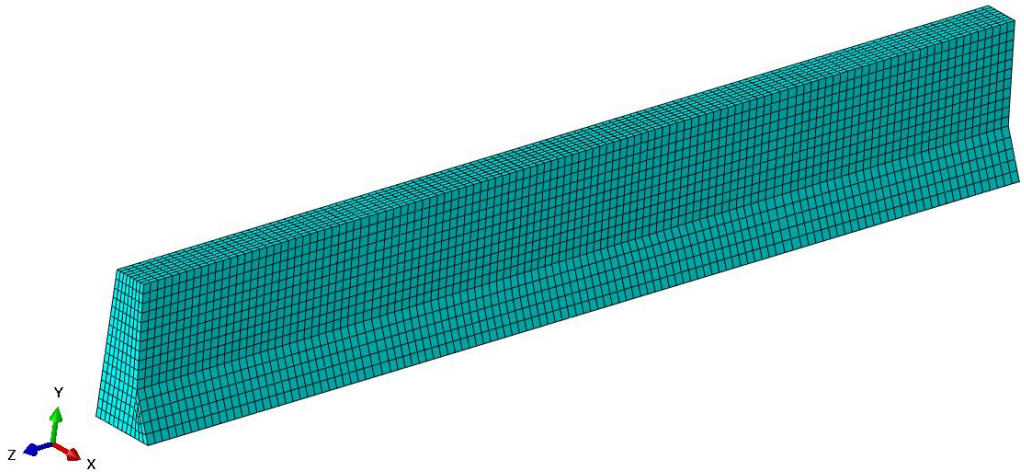

Figure 4.10: Mesh of full barrier model in Abaqus

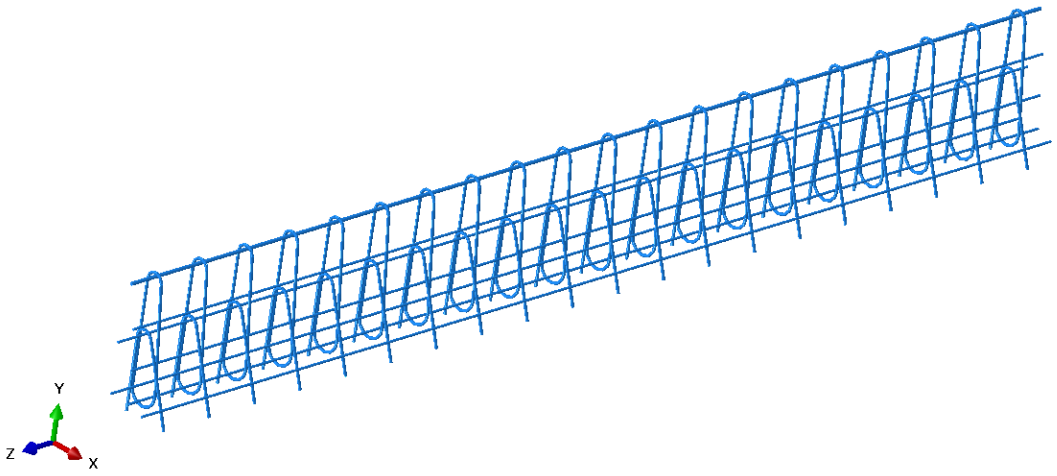

Figure 4.11: Rebar cage in Abaqus

Load was applied evenly across a rectangle covering the top 22” of the barrier and the full length of L_c (Figure 4.12). Concentrated forces along the top edge as used by the yield line analysis not only causes model instability, but also provides a less realistic force distribution compared to a truck impact scenario. A fixed boundary condition was applied on both ends and the bottom of the barrier to closer match the assumptions in the yield line analysis. The barrier was analyzed using Riks arc-length analysis. The most significant difference between the yield line analysis and the FEA is the deformed shape of the barrier (Figures 4.13 and 4.14). While yield line analysis forces the barrier to deform strictly along the yield line pattern, FEA allows the barrier to distribute stress and follow a natural behavior.

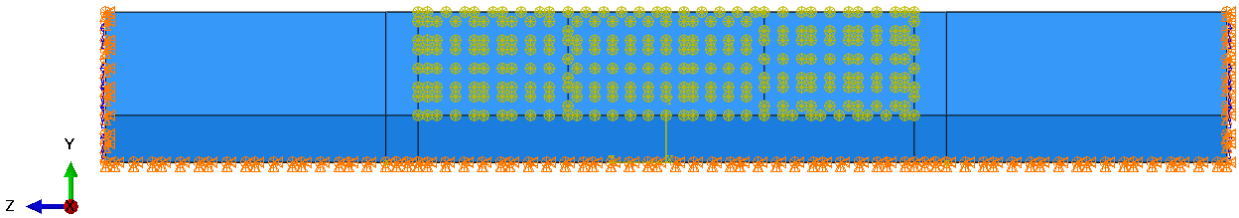

Figure 4.12: Applied load and boundary conditions in Abaqus

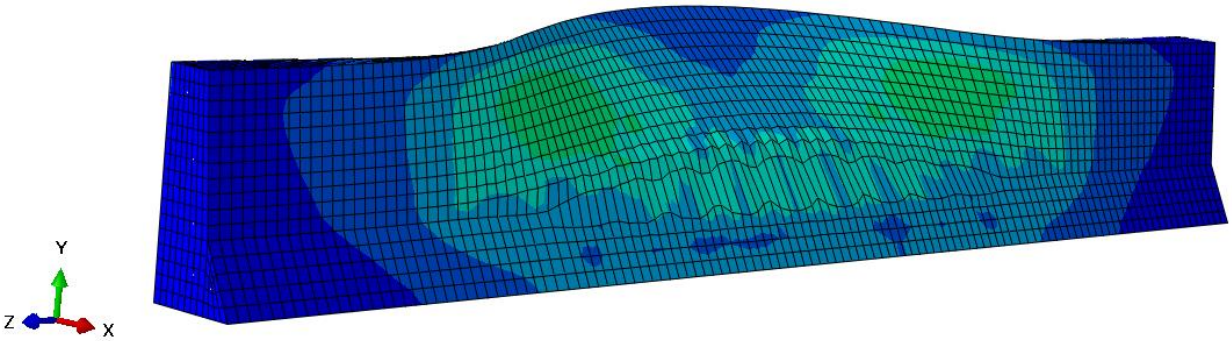

Figure 4.13: Deformed shape of barrier in Abaqus with stress contour

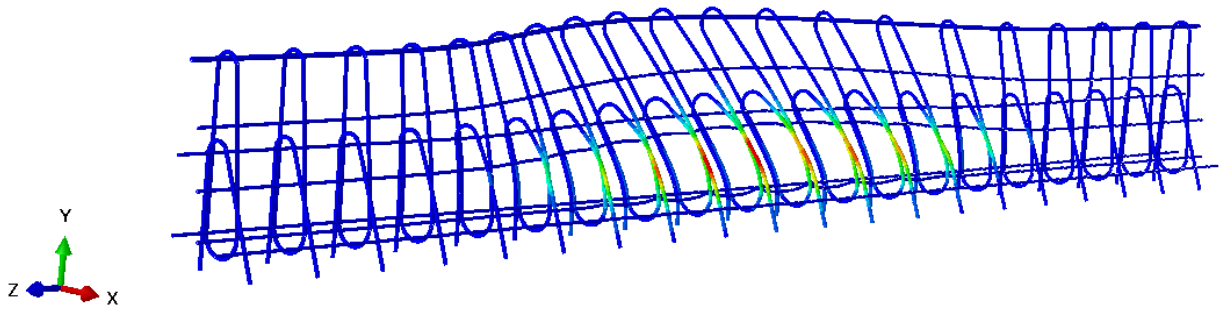

Figure 4.14: Deformed shape of rebar in Abaqus with stress contour

Figure 4.15 shows the load vs displacement for the barrier simulation. Displacement was measured for the top center node on the traffic facing side of the barrier. The maximum load reached was 130.6 kips and the maximum displacement was 0.045 inches. Additionally, the Abaqus model provides the work involved as well. At the maximum load-displacement point, the work performed is 1911 lb-in.

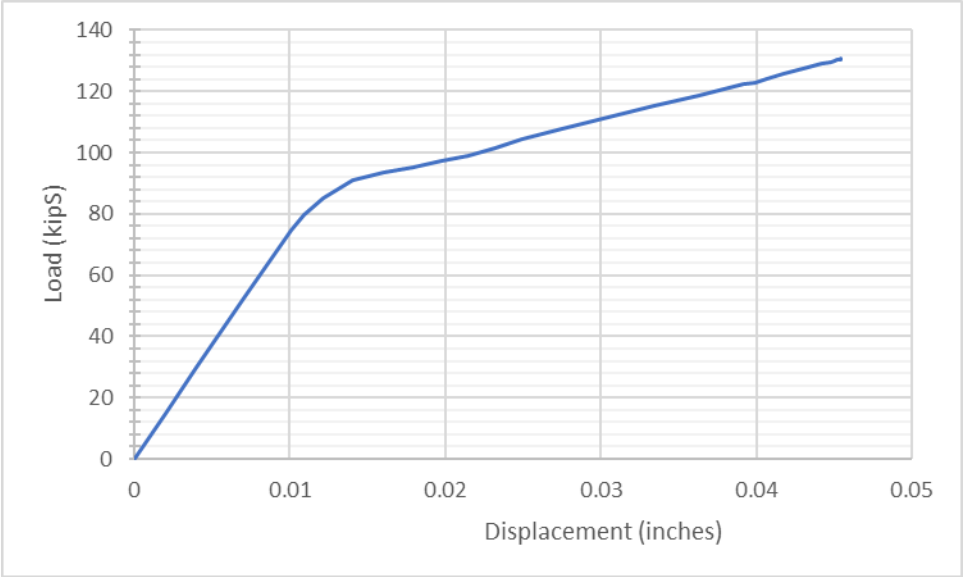

Figure 4.15: Load vs. displacement curve for the full barrier in Abaqus

Comparing the critical load from yield line analysis, 134.8 kips, and the load obtained from Abaqus FEA, 130.6 kips, shows the two analyses strongly agree. A simulation was performed on a slightly modified barrier to compare with these results. The Abaqus model previously described was modified to have a much finer, well-distributed reinforcement cage as assumed in the yield line analysis (Figures 4.16 and 4.17). Bars were reduced in size and spaced at one inch along the lines of average reinforcement depth from Figure 4.5. Stirrups were also reduced in size and spaced at one inch.

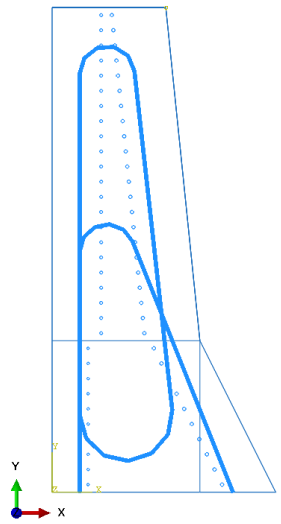

Figure 4.16: Well distributed reinforcement cross-section

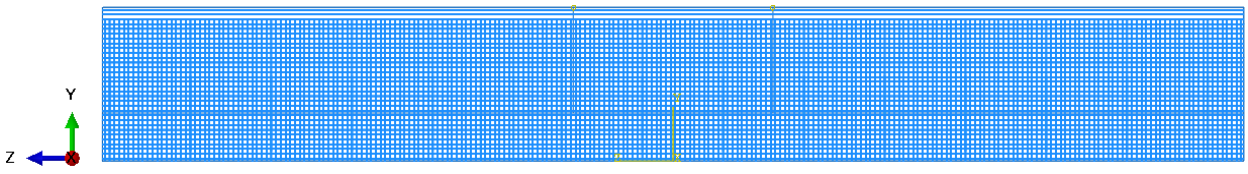

Figure 4.17: Well distributed reinforcement for Abaqus model

The ultimate load reached with the mesh barrier was slightly higher at 142.7 kips with a slightly lower displacement of 0.038 inches, but still very comparable to both the standard model of the barrier and the yield line analysis. This data verifies the results obtained previously. While the work at the point of

failure reaches only 1640 lb-in., these values are low enough that the difference is insignificant in the end result.

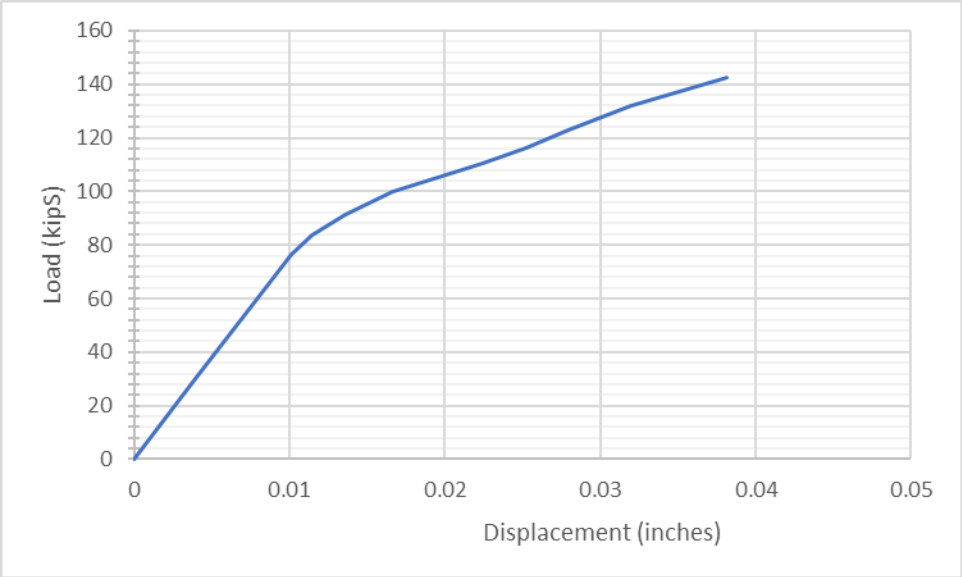

Figure 4.18: Load-Displacement curve for distributed mesh model in Abaqus

One last variation of the full barrier was analyzed to create an envelope. Already discussed was a fully fixed barrier. To investigate the other extreme, a barrier was modeled with the boundary conditions removed for the length of L_c and reapplied at the next set of stirrups outside of that section (Figure 4.19). Figure 4.20 shows the deformed shape and stress contours for the concrete. This variation of the barrier reached a maximum load of only 30.3 kips and the work performed was only 762 lb-in.

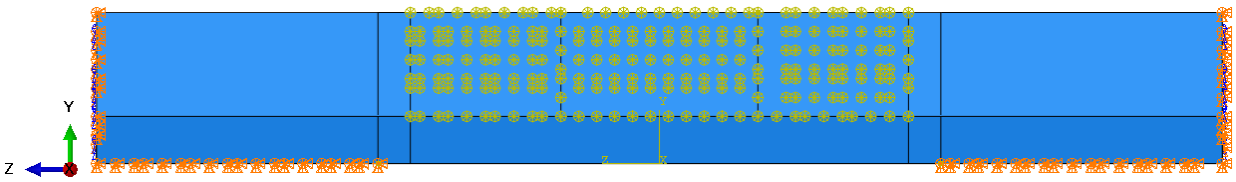

Figure 4.19: Modified barrier with removed boundary conditions

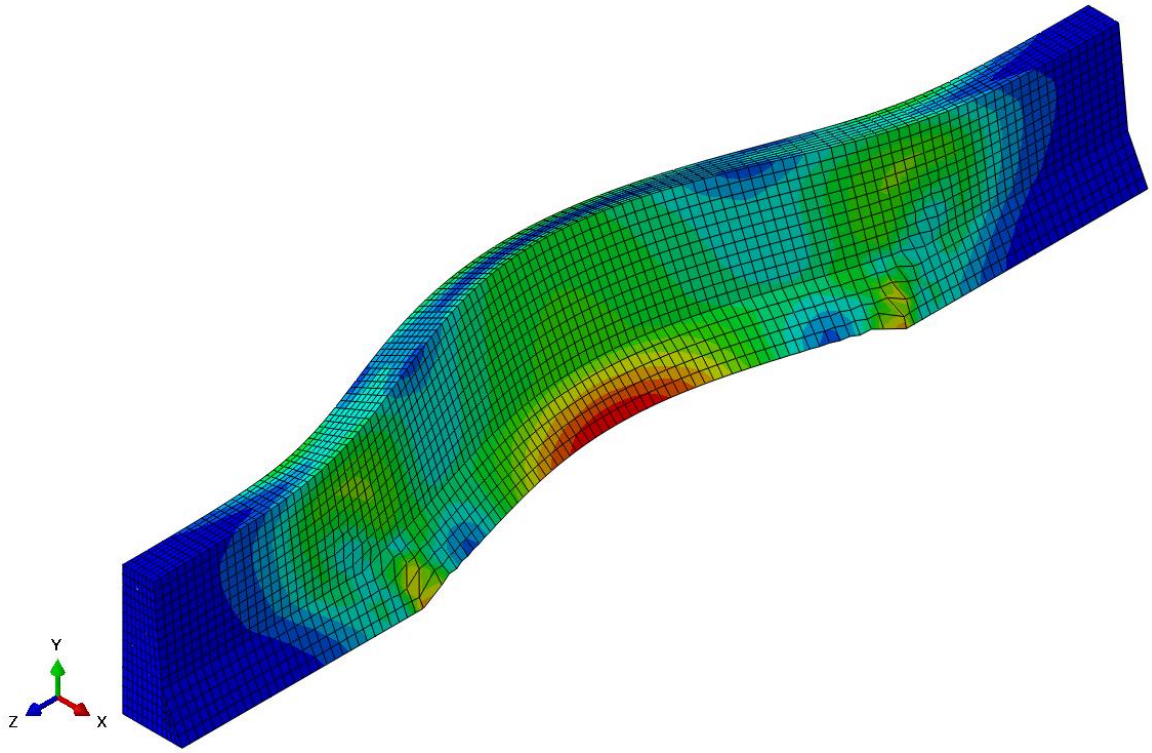

Figure 4.20: Deformed shape of modified barrier with stress contours

Comparing the conditions of Figure 4.12 and 4.19, it can be concluded that the shearing and pull-out strength of the rebar connecting the barrier and pavement has a significant impact on the overall barrier strength. More accurate analysis may be possible with further analysis of these strengths.

Section 4.3: Combined Analysis for Energy

As previously introduced, the energy to break the barrier is only 1911 lb-in. (later referred to as U_1) or 762 lb-in. ($U_{1'}$) if the length of L_c is unconstrained. However, breaking the barrier only accounts for a small amount of the total energy absorbed by the barrier. The next step is actually moving the failed section of the barrier out of the way. Following the assumed yield pattern in Figure 4.1, two triangular pieces of the wall will rotate towards the back side (Figure 4.21) after the load of 134 kips is applied,

from the results of the yield line analysis, until they rest on the ground. A linear load-displacement curve can be created to show that as the sections rotate, the load resistance decreases to zero (Figure 4.22).

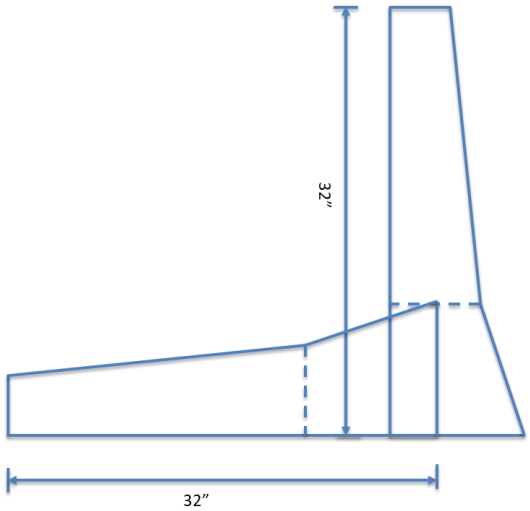

Figure 4.21: Rotation of failed sections of barrier

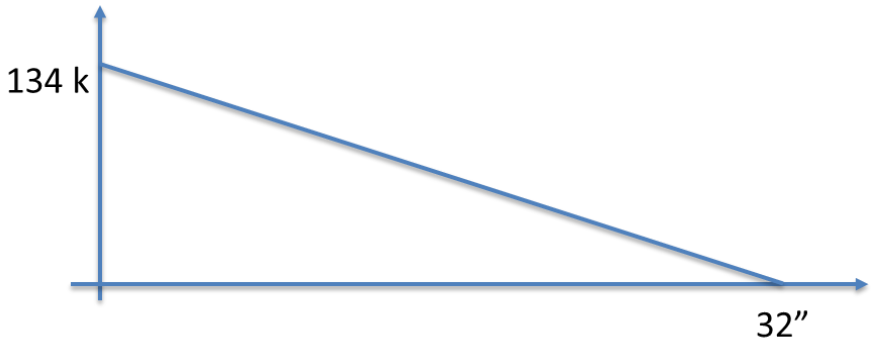

Figure 4.22: Load-displacement curve as failed barrier sections rotate

The work performed by the rotation shown in Figure 4.21 can be calculated as the area under the curve of Figure 4.22. Following that calculation results in an additional energy absorbed by the barrier of 2,144,000 lb-in. (U_2), a much larger amount than the initial formation of the yield lines. This suggests the initial cracking of the barrier only provides a small portion of the total energy absorbed by the barrier.

This does not, however, suggest the strength of the barrier is unimportant as the area under the curve in Figure 4.22 will also decrease with a reduction in the ultimate strength of the barrier.

After the truck pushes through the sections from the original yield line, it will be left with the section shown in Figure 4.23. New yield lines will form along the dashed lines shown.

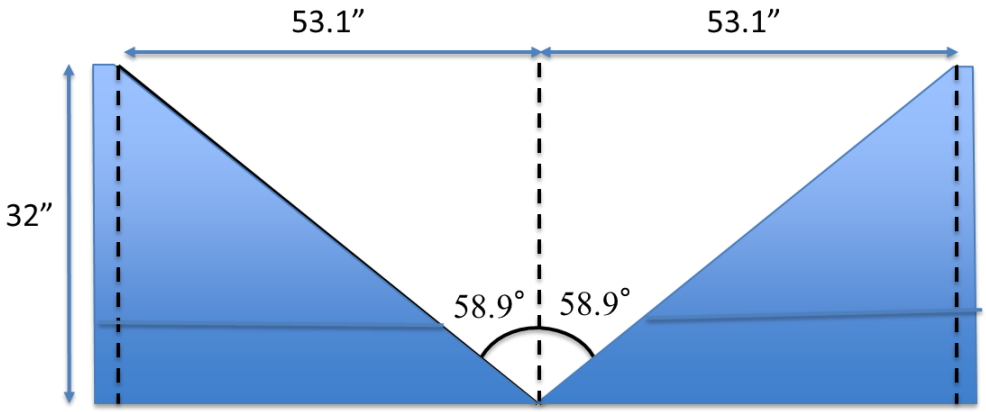

Figure 4.23: Second yield line formation along the dashed lines

For the yield lines to form, the rebar dowels must shear along the bottom of the barrier. With L_c as determined above, nine sets of dowels will be within the yield line when spaced at 12 inches Figure 4.24).

Figure 4.24: Bottom view of barrier showing rebar dowel locations

Using Equation 4.12, the total strength of the dowels is calculated as 150.66 kips.

$$F = 0.45 f_y A_{dowels} = 0.45 \times 60\ ksi \times 9\ sets \times 2\ dowels \times 0.31\ in^2 = 150.66\ kips$$

Equation 4.12

Figure 4.25 depicts the wheel impact represented by a force applied to the second yield line formation. Using yield line analysis for a second time provides the critical force required for the formation of the yield line shown. Equation 4.13 describes the external energy with δ_P defined as the displacement at the location of force, P.

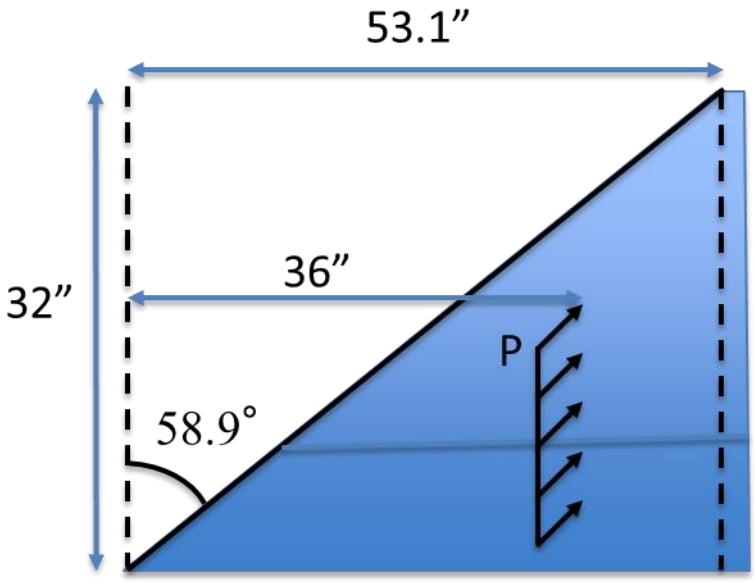

Figure 4.25: Location of wheel force, P, on barrier for second yield line

$$U_{external} = 2\mathrm{P} * \delta_P = 2\mathrm{P}\left[1 - \frac{36"}{L_c/_2}\right] \qquad \text{Equation 4.13}$$

The internal energy (Equation 4.14) will use Equations 4.4 and 4.5 as provided for the original yield line analysis. The resulting internal energy, U_i is 16.66 kip-in.

$$U_{internal} = \int_0^{22} M_{z\_}(z)\, 2\theta(z)\, dz + \int_0^{10} M_{z'\_}(z')\, 2\theta(z')\, dz \qquad \text{Equation 4.14}$$

Combining Equations 4.13 and 4.14, the load, P is found to be 25.86 kips. Due to symmetry of the wheels, the total load is twice P. Adding the resulting 51.7 kips and the result of Equation 4.12, a new load-displacement curve can be formed (Figure 4.26). The maximum displacement will be 53.1" from the triangles hinging around the yield line and being pushed straight back. The area under the curve gives the work done by the process as 5,373,720 lb-in. (U_3). If shearing of the bars is ignored for the section within the yield line, the work done is greatly reduced at only 1,372,635lb-in. ($U_{3'}$).

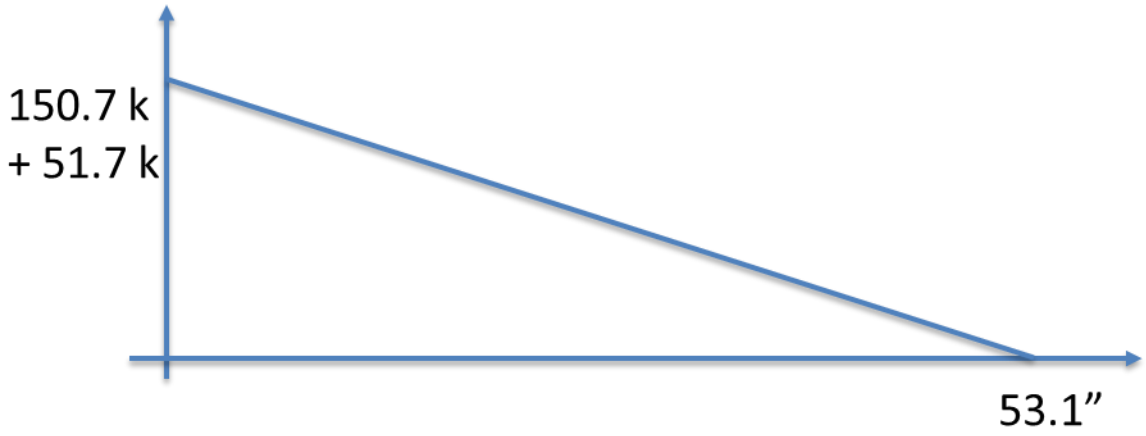

Figure 4.26: Load-displacement curve for second yield line formation

An Abaqus model was also created to verify the maximum force required to yield the barrier along the second yield line formation. The end of the barrier and the bottom were fixed up to the yield line location (Figure 4.27). The triangle section is left free to rotate and a force is applied at the location of the tires.

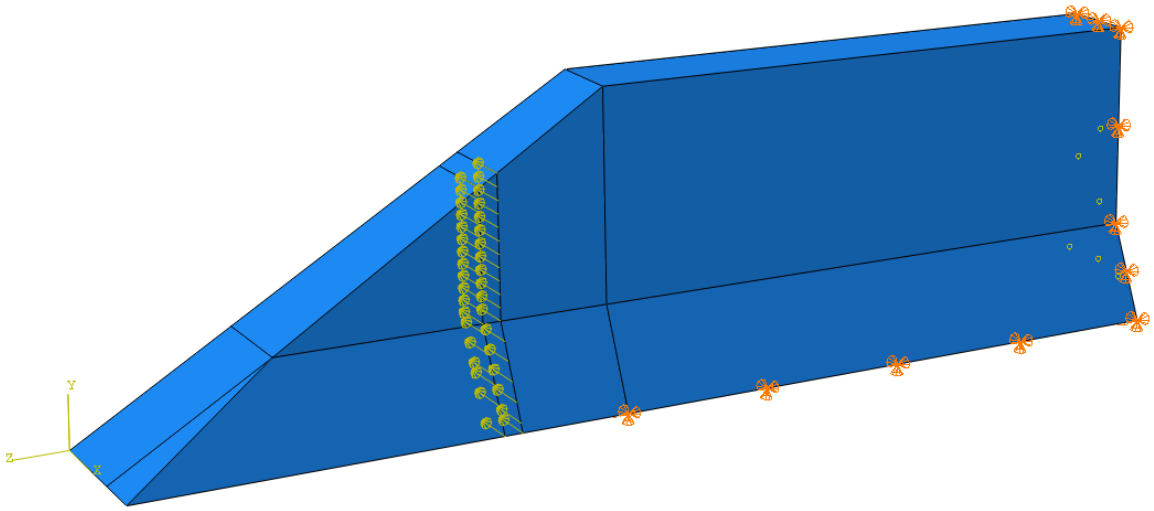

Figure 4.27: Abaqus model to verify force for second yield line formation

The Abaqus model reached a maximum force of only 17.5 kips compared to the 25.9 kips calculated above (Figure 4.28). While a significant discrepancy for this specific step of the calculation, the difference has a minor impact on the overall result. The lower ultimate load obtained from FEA is suspected to be a result of the boundary conditions. With the scenario shown in Figure 4.27, the top vertex of the barrier is allowed to translate and most of the load is transferred through the bottom of the barrier. This causes a higher concentration of stress and lowers the ultimate load because the bottom fails while the top only experiences minimal stress. The yield line analysis, however, evenly distributes the stress across the yield line.

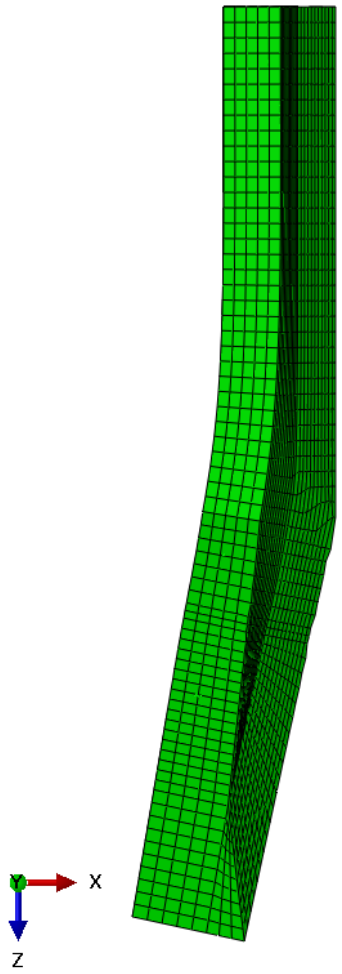

Figure 4.28: Deformed shape of the barrier in the second yield line formation

The final step of the truck overcoming the barrier is the truck driving up onto the barrier as shown in Figure 4.29. For consistency, the weight of the truck is taken as 65 kips from chapter 3 of this report. The base of the barrier is 14.75 inches in thickness, so the energy is the product (Equation 4.15).

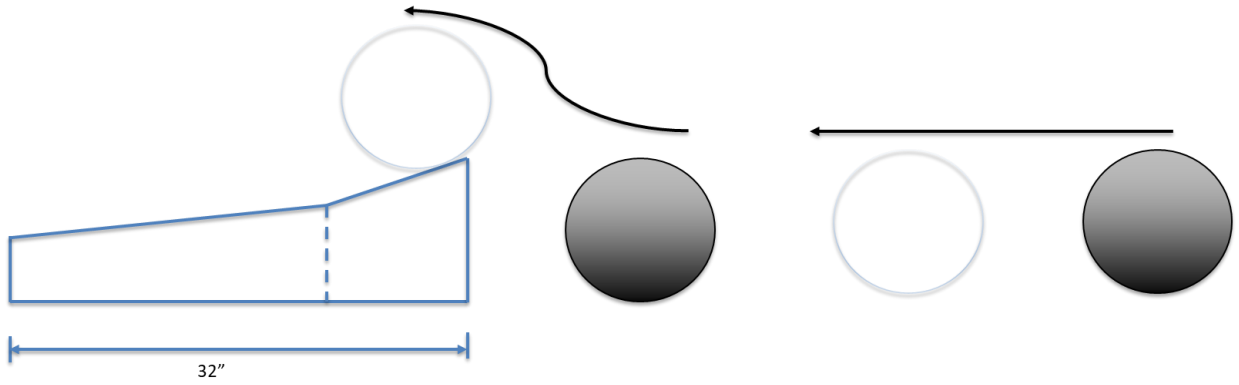

Figure 4.29: Process of the wheels overcoming damaged barrier

$$U_4 = 65000lb \times 14.75" = 958{,}750\ lb - in. \qquad \text{Equation 4.15}$$

By summing the results for all energy components, the total energy absorbed by the barrier is calculated. Equation 4.16 represents the scenario where the rebar must be sheared for the second yield line formation while Equation 4.17, the bars are ignored.

$$U = U_1 + U_2 + U_3 + U_4 = 8{,}478{,}381\ lb - in \qquad \text{Equation 4.16}$$

$$U' = U_1, + U_2 + U_3, + U_4 = 4{,}476{,}147\ lb - in \qquad \text{Equation 4.17}$$

The initial kinetic energy of the truck is given by Equation 4.18.

$$KE_{initial} = \frac{1}{2}\ M\ V^2 = \frac{1}{2} \times \frac{65000\ lb}{32.2 ft/s^2} \times (\frac{73.33 ft}{s})^2 = 65{,}134{,}576\ lb - in \qquad \text{Equation 4.18}$$

For the scenario where the dowel bars must be sheared, Equations 4.19 and 4.20 give the final kinetic energy and velocity.

$$KE_{final} = 65{,}134{,}576\ lb - in - 8{,}478{,}381\ lb - in = 56{,}656{,}195\ lb - in$$

Equation 4.19

$$V_{final} = \sqrt{\frac{56{,}656{,}195 \times 64.4}{12 \times 65000}} = 68.39 \frac{ft}{s} = 46.6 mph$$ Equation 4.20

For the scenario where the dowel bars are ignored, Equations 4.21 and 4.22 give the final kinetic energy and velocity.

$$KE_{final} = 65{,}134{,}576\ lb - in - 4{,}476{,}147\ lb - in = 60{,}658{,}429\ lb - in$$

Equation 4.21

$$V_{final} = \sqrt{\frac{60{,}658{,}429 \times 64.4}{12 \times 65000}} = 70.77 \frac{ft}{s} = 48.3 mph$$ Equation 4.22

While the results may first appear insignificant, these values are for the truck impacting at 90°. This is both the worst case scenario and the most unlikely to occur.

Chapter 5: Conclusion

The research discussed in Section 3.1 show that the impact target plays a particularly important role in the force time curve generated from the impact. As the column used by the TTI research team was extremely stiff, this could suggest the design requirement of 600 kips is a conservative value before protective barriers are even considered. Further analysis of the forces experienced without a protective barrier has the potential to show a force lower than 600 kips is appropriate.

The results for the effects of a barrier are similar between the two analysis approaches, transient dynamic FEA and yield line combined with static FEA. The results are summarized in Table 5.1. All results show a reduction of only a few mph in velocity and all energy reductions are on the same order of magnitude. With the small magnitudes of change for the 90° approach angle and initial velocity of 50 mph, a small discrepancy can appear as a large error. However, when considering the results from the other transient dynamic simulations, the results are promising and support each other.

Table 5.1: Summary comparison of two analysis approaches

90° 50 mph		Yield Line/Static FEA	Transient Dynamic FEA
Fixed	Velocity Reduction (mph)	3.4	2.4
	KE Reduction (lb-in)	8.48×10^6	5.01×10^6
Free	Velocity Reduction (mph)	1.7	3.2
	KE Reduction (lb-in)	4.48×10^6	6.92×10^6

The results of this study show that for a large truck such as the f800 used in Chapter 3, the reduction in energy may be significant for most situations. The high angles of approach are much less likely to occur than the lower angles according to outside research and the data introduced by this study shows that the barrier is highly effective with lower angles of approach.

Chapter 6: Suggestions for Phase 2

Phase 2 of this project has the ability to improve on many of the parameters used in this thesis. Perhaps the most important is the vehicle model used in the transient dynamic simulations. As previously discussed, the design specifications provided by AASHTO are based on the results from an 80 kip tractor-trailer truck. Vehicle dynamics play an important role in the force-time curves and the resulting damage to the barrier and column. For a more confident reduction of the design force in AASHTO's specification, the model should match the original vehicle in both shape and weight. Material models also play a significant role in the simulations and should be refined for phase 2. Improvements will require experimental testing of samples to calibrate the material properties but will, again, raise the confidence of the simulations.

The yield line analysis used in this study only applies to perpendicular loading. Development of an approach for various angles would provide a wider data set and perhaps a tool for industry use. Additionally, adapting yield line theory to provide better approximations of the energy would benefit analysis of existing barriers as well as the design of new barriers. The final recommendation for phase 2 is the investigation of barrier optimization, a slightly modified design may provide significantly more protection for the bridge piers.

Bibliography

[1] American Association of State Highway and Transportation Officials (AASHTO), Washington, DC, USA. *AASHTO LRFD Bridge Design Specifications*, 8th Edition (2017). Accessed: Sep. 2019. [Online]. Available: https://app.knovel.com/hotlink/toc/id:kpAASHTO94/aashto-lrfd-bridge-design/aashto-lrfd-bridge-design

[2] E. Buth et al., "Analysis of large truck collisions with bridge piers: phase 1. Report of guidelines for designing bridge piers and abutments for vehicle collisions," Texas Transportation Institute, The Texas A&M University System, College Station, Texas, USA, Rep. FHWA/TX-10/9-4973-1, 2010

[3] E. Buth, M. S. Brackin, W. F. Williams and G. T. Fry, "Collision loads on bridge piers: phase 2. Report of guidelines for designing bridge piers and abutments for vehicle collisions," Texas Transportation Institute Proving Ground, The Texas A&M University System, College Station, Texas, USA, Rep. FHWA/TX-11/9-4973-2, 2011

[4] M. F. B. M. Zain, H. J. Mohammed, "Concrete road barriers subjected to impact load: An overview," *Latin American Journal of Solids and Structures*, vol. 12, no. 10, pp. 1824-1858, Oct. 2015. doi: 10.1590/1679-78251783.

[5] A. Badiee, "Dynamic simulation of concrete barriers," M.S. Thesis, Civil Engineering, The University of Alabama at Birmingham, Birmingham, Alabama, USA, 2015. [Online]. Available: https://er.lib.k-state.edu/login?url=https://search-proquest-com.er.lib.k-state.edu/docview/1749282125?accountid=11789

[6] B. R. Calloway, "Yield line analysis of an AASHTO new jersey concrete parapet wall," M.S. Thesis, Civil Engineering, Virginia Polytechnic Institute and State University, Blacksburg, Virginia, USA, 1993. [Online]. Available: https://vtechworks.lib.vt.edu/handle/10919/34936

[7] *AASHTO Standard Specifications for Highway Bridges*, American Association of State Highway and Transportation Officials (AASHTO), Washington, DC, USA, 1992.

[8] *AASHTO LRFD Bridge Design Specifications, 1st Edition*, American Association of State Highway and Transportation Officials (AASHTO), Washington, DC, USA, 1994.

[9] T. J. Hirsch and W. L. Fairbanks, "Bridge Rail to Contain and Redirect 80,000-lb Tank Trucks," Transportation Research Board, National Research Council, Washington, DC, USA, Record No. 1024, (1985).

[10] National Cooperative Highway Research Program (NCHRP), "Guidelines for Shielding Bridge Piers," National Academy of Sciences, Engineering, and Medicine, Washington, DC, USA, Report 892, (2018).

[11] American Association of State Highway and Transportation Officials (AASHTO), Washington, DC, USA. *AASHTO LRFD Bridge Design Specifications*, 6th Edition (2012).

[12] National Cooperative Highway Research Program (NCHRP), "Recommended Procedures for the Safety Performance Evaluation of Highway Appurtenances," National Academy of Sciences, Engineering, and Medicine, Washington, DC, USA, Report 230, (1981).

[13] National Cooperative Highway Research Program (NCHRP), "Recommended Procedures for the Safety Performance Evaluation of Highway Features," National Academy of Sciences, Engineering, and Medicine, Washington, DC, USA, Report 350, (1993).

[14] *Manual for Assessing Safety Hardware*, 6th Edition. American Association of State Highway and Transportation Officials (AASHTO), Technical Committee for Roadside Safety, Washington, DC, USA. 2012.

[15] "F800 Single Unit Truck FEM Model for Crash Simulations with LS-DYNA." National Transportation Research Center, Inc. https://thyme.ornl.gov/FHWA/F800WebPage/downloads/downloads.html (accessed December, 2019).

[16] Livermore Software Technology Corp., Livermore, California, USA. *LS-DYNA Keyword User's Manual*, Version 971 (2007). Accessed: Dec., 2019. [Online]. Available: http://lstc.com/pdf/ls-dyna_971_manual_k.pdf

[17] F. Lin, Y. Dong, X. Kuang, L. Lu, "Strain Rate Behavior in Tension of Reinforcing Steels HPB235, HRB335, HRB400, and HRB500," *Materials*, Vol. 9, Issue 12, December 2016, doi:10.3390/ma9121013

[18] Dassault Systèmes, Providence, RI, USA. *Abaqus/CAE User's Guide*, (2019). Accessed: Sep. 2019. [Online]. Available: https://help.3ds.com/2019/English/DSSIMULIA_Established/SIMULIA_Established_FrontmatterMap/sim-r-DSDocAbaqus.htm?ContextScope=all&id=6e37335455a1420f9de68129400a122c#Pg0

[19] *Building Code Requirements for Structural Concrete*, (ACI 318-19), American Concrete Institute (ACI), Farmington Hills, MI, USA, (2019).

[20] S. V. Chaudhari, M. A. Chakrabarti, "Modeling of concrete for nonlinear analysis using finite element code Abaqus," *International Journal of Computer Applications*, Volume 44, No. 7, April 2012